JRC TECHNICAL REPORTS

Non destructive characterization of oxide dispersion strengthened steels

Vladimir Kršjak, Zoltan Szaraz,
Jozef Snopek, Peter Haehner

2012

Report EUR 25266 EN

European Commission
Joint Research Centre
Institute for Energy and Transport

Contact information
Peter Haehner
Address: Institute for Energy and Transport, P.O. Box 2, NL-1755 ZG, Petten, The Netherlands
E-mail: peter.haehner@ec.europa.eu
Tel.: +31 224 56 5217
Fax: +31 224 56 5627

http://iet.jrc.ec.europa.eu/
http://www.jrc.ec.europa.eu/

JRC69660

EUR 25266 EN

ISBN 978-92-79-23552-8 (pdf)
ISBN 978-92-79-23551-1 (print)

ISSN 1831-9424 (online)
ISSN 1018-5593 (print)

doi: 10.2790/46588 (online)

Luxembourg: Publications Office of the European Union, 2012

Printed in Netherlands

Content

1. Introduction

Next generation nuclear power installations require new nuclear structural materials. New types of coolants, elevated operating temperatures, different neutron spectra and considerably higher end-of-lifetime fluencies require high performance materials which are costly or, still have to be developed and qualified. Even for already existing materials, developed for particular applications and exhibiting promising irradiation performance under high neutron dose exposure (e.g. 9-12%Cr ferritic/martensitic steel, 16-20%Cr ODS steel [1]), micro-structural properties may still not be sufficiently understood to reliably predict their long term behaviour in the above mentioned conditions.

More and more experimental techniques are being used in materials research in order to understand the effect of particular alloying elements, impurities and various nano-features on irradiation performance. Although many papers have been published on the application of (thermo) electric, magnetic, ultrasound or diffraction based techniques to radiation embrittlement studies [2-6], the connection between these techniques is missing. This can result in the underestimation of the potential contribution of the particular method or the lack of a link between the measured parameter and the actual microstructure state.

This report discuss the application of various non-destructive testing methods on the microstructural characterization of nano-structured ferritic alloys (ODS steels) for nuclear applications. Emphasis is put on a multi-technique approach and mutual correlation of results as well as on the validation and interpretation of the results obtained by destructive mechanical tests. Results presented in the report are of the fundamental importance for future irradiation experiments, foreseen in the frame of international joint research activities (e.g. FP7-project GETMAT).

Most of the experiments presented in this report were conducted in order to study so called 475°C embrittlement. This is an important material performance problem, which significantly change the tensile, fracture and fatigue behaviour of the high Cr steels (>12 wt%). It is accompanied by decomposition of the ferritic phase to chromium-rich phase α' and iron-rich phase α in the temperature range of 280–500 ◦C due to the presence of miscibility gap in iron–chromium binary alloy system, resulting in embrittlement of the microstructure [7]. In this report, the results of positron lifetime spectroscopy (PALS), small angle neutron scattering (SANS), thermoelectric power measurements (TEP) and magnetic Barkhausen noise (BN) measurements on the thermally aged materials are discussed. Interpretation of the results was based on the previous published papers on nuclear structural materials as well as on the preliminary TEM experiments performed in the collaboration with Nuclear Research Centre Negev, Israel.

2. Materials

Oxide dispersion strengthened steels (ODS) have been developed for high temperature applications like heat exchangers in conventional power plants. In addition to superior creep properties at temperatures up to 1200°C these materials generally show excellent corrosion and swelling resistance when irradiated by neutrons [1], which suggests their application in future nuclear reactor systems. The combination of elevated temperatures, high pressures, new coolant environments and considerably higher displacement damage, together with general requirements for outstanding passive safety features, necessitates extensive R&D efforts including advanced microstructural characterization techniques.
The objects of our study were various oxide-dispersion strengthened (ODS) steels, namely PM2000, MA956, MA957 and ODM751 as well as ODS variant of Eurofer steel. Chemical compositions of the studied materials are listed in Table 2.1. These materials are strong candidates for structural materials used in Generation IV reactors which have to endure extreme service conditions. Service conditions that characterize these reactors include:

1. operating temperature above 700°C
2. high neutron doses
3. highly corrosive environment

Table 2.1 shows the nominal compositions of commercially available ODS steels [8] investigated by PALS in the present work. Ferritic PM2000 steel has been supplied in both as-extruded and recrystallized conditions. MA957 and an ODS variant of ferritic-martensitic EUROFER steel have been supplied in as-extruded condition and the ferritic alloys ODM751 and MA956 were available in recrystallized condition only. As for the reference, non-ODS Eurofer 97 steel was included in the sample set.

Table 2.1 – Nominal chemical compositions [wt%] of the materials studied

Material	Form	Manufacturer	Cr	Al	Ti	Mo	W	Mn	V	Y_2O_3
PM2000	1, 2	Plansee	20	5.5	0.5	-	-	-	-	0.5
MA956	2	INCO	20	4.5	0.5	-	-	-	-	0.5
ODM751	2	Dour Metal	16.5	4.5	0.6	1.5	-	-	-	0.5
MA957	1	INCO	14	-	0.9	0.3	-	-	-	0.25
(ODS) Eurofer	1	Plansee	8.9	-	-	-	1.1	0.4	0.2	(0.3)

Form: 1 - as extruded; 2 –recrystallized

The microstructures of the as-extruded materials can be described as fine grained with high dislocation densities and with complex microstructures [8]. Recrystallization annealing (typically at ~$0.9T_{melt}$) of the ODS steels leads to very coarse grain structures with exceptional creep resistance. In the process of recrystallization, very fine oxide particles in the diameter range 2 to 5 nm dissolve or coarsen while the number of larger dispersoids (15 – 40 nm) increases, thus resulting in larger mean diameters of the oxide nano-particle size distributions [8 - 11]. Basic characteristics of the mean particle size and concentration of the studied materials, obtained from the literature, can be seen in Table 2.2.

Table 2.2 – Basic characteristics of the oxide nanoparticles adopted from literature

Material	Average particle size [nm] as extruded / recrystallized	Particle concentration [10^{22} m^{-3}] as extruded / recrystallized	Reference
PM2000	12 / 28	0.64[1] / 0.05	[8, 10]
MA956	- / 28	- / 0.05	[8, 10]
ODM751	- / 28	- / 0.05	[11]
MA957	3 / -	6.6 / -	[12]
ODS Eurofer	9 / -	1.1 / -	[13]

In order to induce the intermediate temperature embrittlement, all recrystallized samples as well as ODS Eurofer have undergone isothermal annealing treatment at 475°C for 100, 500 and 1000h in high temperature furnace, LECO HT 1600, under Ar atmosphere of 5 mBar overpressure. At this temperature a phase separation of ferrite phase into Fe-rich α and Cr-rich α' phase occurs. The reason of this so called 475 °C embrittlement phenomenon is the miscibility gap in the Fe-Cr equilibrium system [14].
In order to distinguish the effect of α'precipitation from other thermal annealing effects, analogical thermal aging at 650°C was performed. Phase separation at this temperature does not take place and material generally does not suffer from embrittlement.

[1] Concentrations after recrystallization were calculated from the known particle size by assuming the total volume fraction (average particle volume × concentration) of the yttria particles to be constant i.e. oxides are chemically stable at the recrystallization temperature and the coarsening of the particles is accompanied by equivalent reduction of the concentration.

3. Experimental techniques

Promising irradiation performance of the new generation of materials strengthened by the dispersions of oxide nanoparticles is offset by a material microstructure which is too complex to be captured by numerical simulations. Moreover these materials are typically strongly anisotropic, which complicates the sampling of the representative specimens for Transmission Electron Microscopy (TEM) and Atom Probe (AP) analysis. Therefore, the key motivation to our study was to overcome the material anisotropy by investigation of sufficiently large representative volumes with sufficiently sensitive methods in order to understand the role of individual nano-features in the material performance in operation and/or transition regimes.
In principle, the particular defects can act as e.g. trapping sites for positrons, scattering centre for neutrons, pinning sites for magnetic domain movement and at the same time significantly affect the material's electronic properties. Consequently, several experimental techniques based on different physical principles can be combined in an effort to obtain specific information. This chapter discus the application of four experimental techniques on the microstructural characterization of oxide dispersion strengthened steels:

3.1. Positron annihilation lifetime spectroscopy (PALS)

Positron annihilation lifetime spectroscopy (PALS) is a non-destructive testing method widely used in the solid state physics. This technique is extremely sensitive to atomic-scale defects in solids, like vacancies, their agglomerates or dislocations. In addition thermalized positrons are sensitive to (as they may be trapped in) precipitates of elements with higher (more negative) positron affinity (A^+) than the bulk material. For example this holds true for ODS steels, where yttrium (positron affinity A^+ = -5.31) oxides are being used as obstacles for dislocation motion in Fe-Cr matrix (A^+ of Fe and Cr = -3.84 and -2.62 respectively [15]). In this study, the PALS technique was used for the characterization of vacancy type defects in the studied ODS alloys, both in the as-extruded and the as-recrystallized state. Although the positron lifetime technique is not directly sensitive to the Cr-rich α' precipitates we use this technique in the study of thermally aged materials in order to obtain a complementary information on the behaviour of vacancy type defects, which are mobile at this temperature and they play a role in the material performance.
Schematic representation of the used lifetime spectrometer in so called fast - fast setup is shown in the Fig. 3.1.1. It is based on the universal NIM blocks of Canberra and Ortec suppliers and its resolution is < 220ps. The BaF_2 scintillation detectors were fabricated and supplied by Scionix together with the HV dividers. The whole experimental facility is shown in the Fig. 3.1.2 (left).

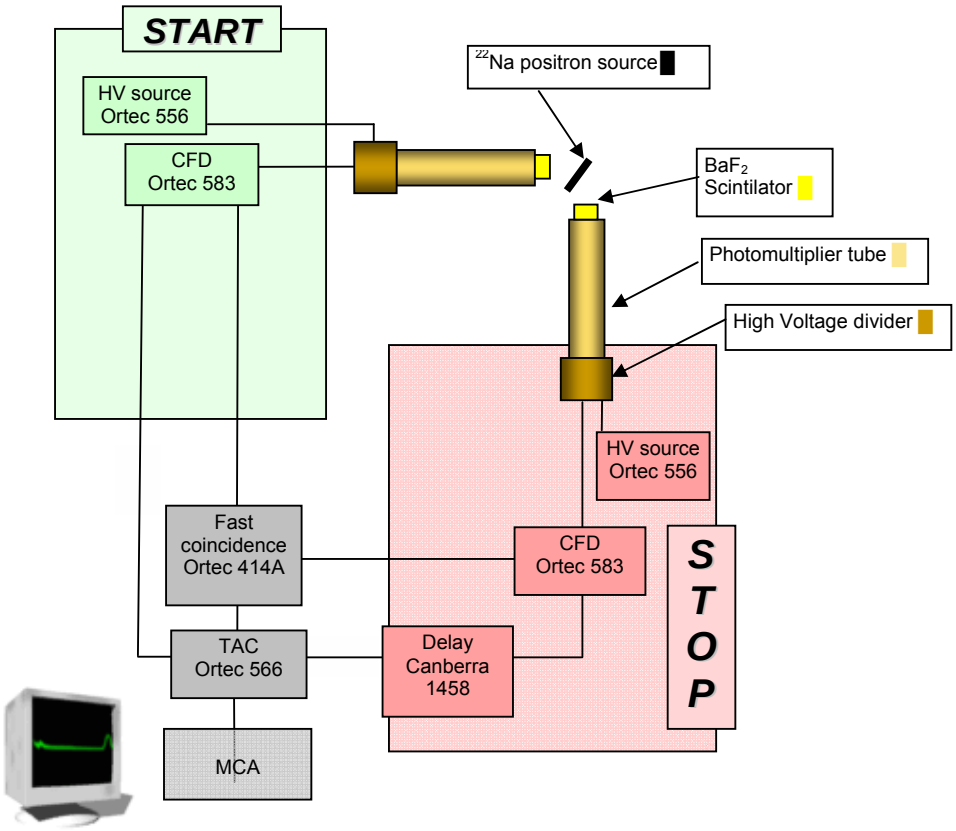

Fig. 3.1.1. Scheme of the setup for the measurement of positron lifetime at JRC-IET.

Positron source used for the experiments is shown in the Fig. 3.1.2 (right). It is a ^{22}Na positron source, with active diameter of 6mm, encapsulated in kapton foil. Source was purchased from external supplier and its activity > 3MBq allowed us to obtain sufficient spectrum (10^6 counts) within few hours. Source contribution to the final lifetime spectra (13%) was described by two components (382ps/60% and 1300ps/40%) and fixed during the data processing. Time resolution function of the experimental facility was described by 220ps wide Gaussian.

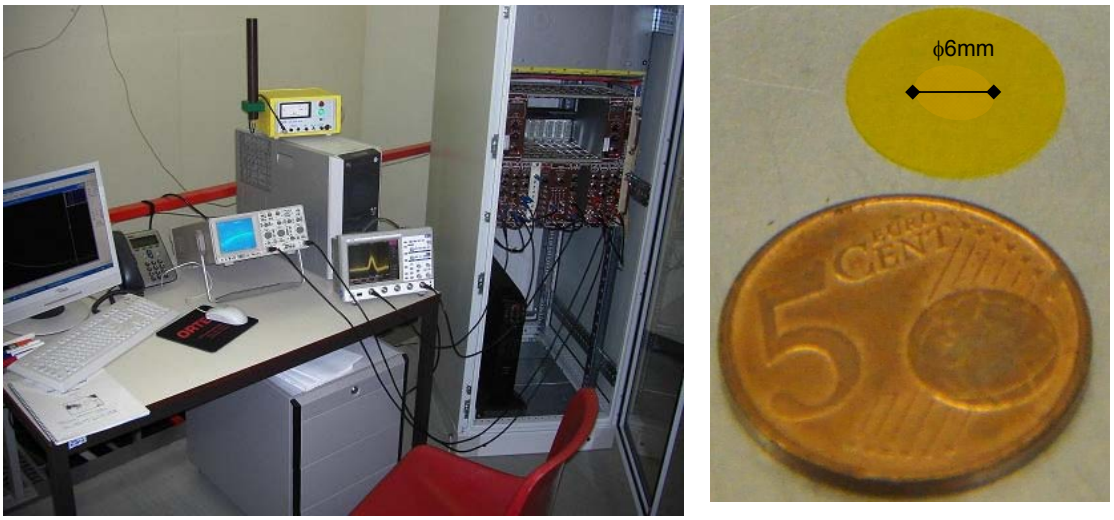

Fig. 3.1.2. Experimental facility (left) and the used positron source (right).

3.2. Small angle neutron scattering (SANS)

Small-Angle Neutron Scattering (SANS) is a method for analyzing materials inhomogeneities in the range of 1-100 nm. Neutrons, being neutral particles, interact weakly with matter which allows probing specimens of considerable thickness. In SANS experiments volumes up to 1 cm^3 are investigated. SANS determines the differential cross-section, which contains the information on the shape, size and interactions of the scattering bodies in the sample. This method can be used to study effects of thermal and/or irradiation ageing in ODS, duplex or Cr rich ferritic steels.

The neutron scattering lengths vary with atomic number more or less randomly and are independent of momentum transfer q. Thus, isotopes and neighbouring elements can possess different scattering properties. SANS is particularly powerful in the case of study the α' phase separation because of the large difference between the neutron coherent scattering lengths of Fe (9.45×10^{-15} m) and Cr (3.635×10^{-15} m).

The Small-Angle Neutron-Scattering (SANS) facility at the 45MW High-Flux Reactor in Petten, is located at beam tube HB3b. The instrument has a length of approximately 10 meters. Scheme of the facility is shown on figure 3.2.1. It is a medium size SANS instrument covering a q range of 5×10^{-3} – 0.4 $Å^{-1}$. A double crystal pyrolytic graphite monochromator selects from a neutron spectrum a band corresponding to an average wavelength of 4.75 Å of a width $\Delta\lambda/\lambda$ = 10%. A cooled Be filter is placed close to the monochromator to suppress higher-order contamination. The flux at the sample position in the current setup is $\sim 10^4$ $n.cm^{-2}.s^{-1}$. The distance between the sample and the two dimensional detector, filled with ^{3}He-detection gas, can be varied continuously from 0.9 to 4.25 m. All components of the flight path can be evacuated in order to reduce attenuation through air scattering.

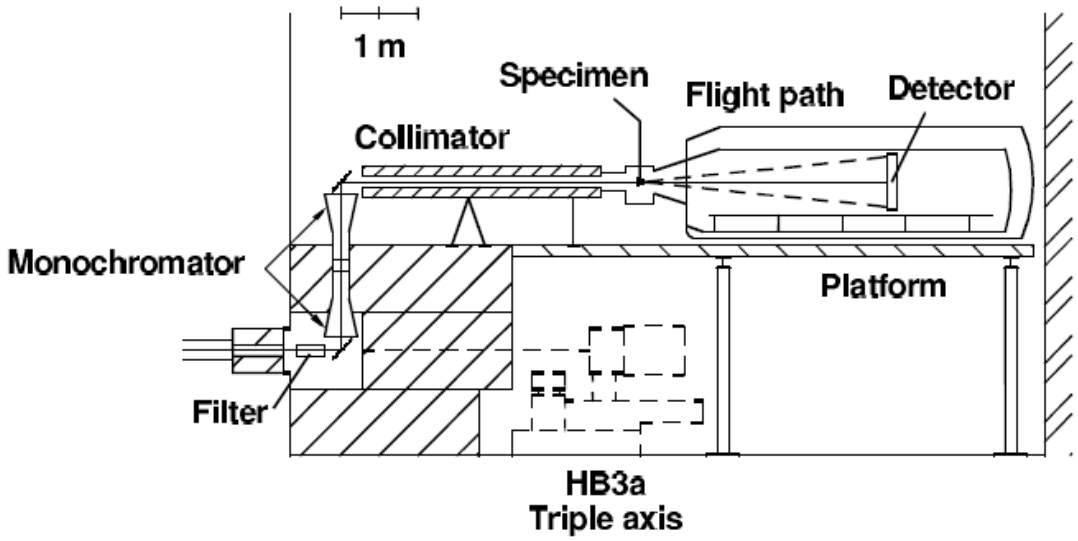

Fig. 3.2.1 Scheme of the small-angle neutron scattering facility at the high flux reactor (HFR) Petten.

3.3. *Thermoelectric power measurements (TEP)*

Measuring of thermoelectric power (TEP) is based on the Seebeck effect. If two different conductors are joined and the two junctions are maintained at different temperatures, an electromotive force ΔE is developed in the circuit. The generated voltage is generally proportional to the temperature difference ΔT between the two junctions. The ratio ΔE/ΔT is the Seebeck coefficient (S).

Experimental device for the TEP measurements consists of two copper blocks, on top of which the specimen to measure is placed (Fig. 3.3.1). Temperature gradient across the sample (when one of the blocks is heated) induces thermoelectric voltage between sample's tips. During the measurements (~2min) both temperature difference and thermoelectric voltage (ΔE) are recorded and the thermoelectric power is obtained as the slope of the ΔE - ΔT curve. The Seebeck coefficient measured in this way is the Seebeck coefficient of the sample relative to copper. A typical uncertainty of these measurements is 3%. Our TEP device has been constructed for the measurements of small samples where the dimensions can be in the range from 10x10mm (here the maximum - diagonal distance is used) up to Charpy samples. Device is portable and is suitable for the measurements of irradiated samples in hot cells. The main advantage of the techniques is the simplicity of apparatus and excellent repeatability of results. However the results of these experiments must be interpreted very carefully and with respect to complementary information derived by other analytical techniques.

The Seebeck coefficient depends on the chemical composition and the microstructure of the conductor. Thermal ageing and neutron irradiation can change the thermoelectric power of metals and alloys. This change can be correlated to the change in the microstructure and the mechanical properties of the treated materials. TEP measurements have been successfully applied to radiation embrittlement and ageing studies [16, 17].

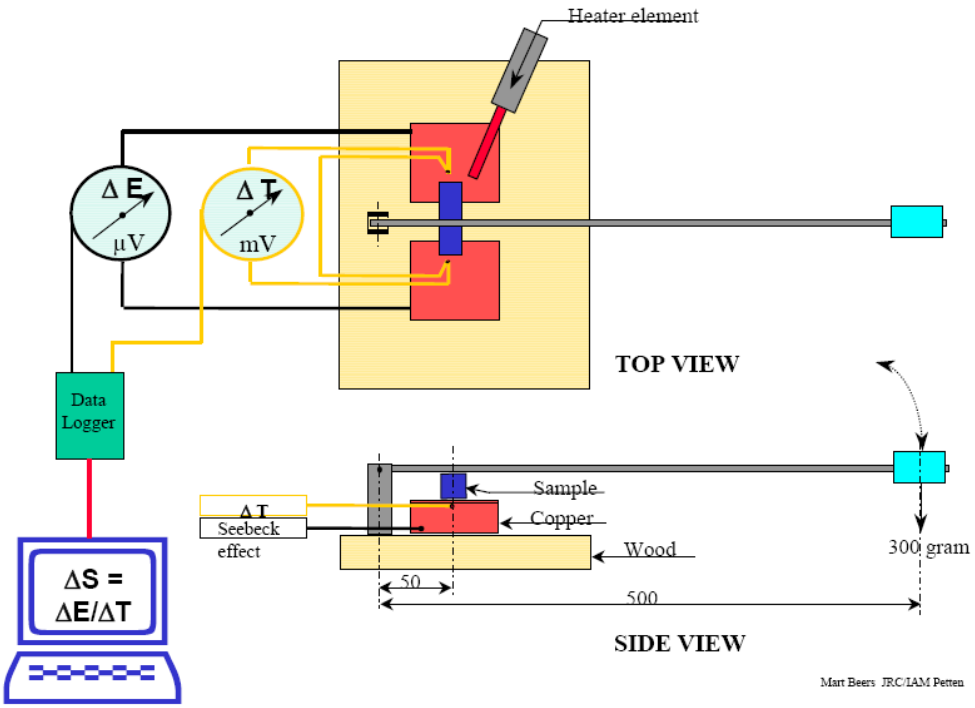

Fig. 3.3.1. Scheme of the TEP device for material characterization.

3.4. Magnetic Barkhausen Noise technique

Magnetic Barkhausen Noise (BN) analysis is based on a concept of inductive measurement of a noise-like signal, generated when magnetic field is applied to a ferromagnetic sample. Barkhausen technique is a valuable experimental tool because of its capability to characterise materials properties accurately, easily, quickly and in non-destructive way. Magnetic Barkhausen Noise (BN) is considered as an important technique for microstructural and mechanical characterization of ferromagnetic materials like steels. The main advantage of this method is its non-destructive character and variety of sensors enabling to investigate various shapes and sizes of samples. BN is sensitive to various parameters which affect the magnetic domains configuration and domain-wall pinning sites. These parameters are particularly grain size, chemical composition, different phase precipitates, surface conditions, hardness, residual stress and fatigue but also by magnetic field strength and applied stress [18, 19]. In addition to the industrial application (aviation, pipeline transport, automobile industry) [20, 21], this technique can be well used for the material performance assessment of the nuclear installations [22].

Magnetic Barkhausen noise has a power spectrum starting from the magnetizing frequency and extending beyond 2 MHz in most materials. It is exponentially damped as a function of distance it has travelled inside the material. This is primarily due to the eddy current damping experienced by the propagating electromagnetic fields that domain wall movements create. The extent of damping determines the depth from which information can be obtained (measurement depth). The main factors affecting this depth are frequency range of the Barkhausen noise signal analyzed, conductivity and permeability of the test material. Measurement depths for practical applications vary between 1 and 30 mm.

In our experiments commercially available measuring device μScan 500 V.C3.0 manufactured by Stresstech group was used. Magnetizing coil was build together with pick-up coil in sensor (μScan) provided by the same manufacturer (Fig. 3.4.1).

Fig. 3.4.1. Microcomputer based signal analyzer μSCAN 500C (left) and sensor (right) used in the experiments.

The major challenge associated with the application of BN technique in material research is that no commonly accepted standard for the measurements has yet been established. This complicates the correlation of data between experiments and weakens the potential contribution of this technique to material research. In order to understand the material response and to enable future application of this technique on the investigation of irradiated materials, we have conducted series of measurements with different setup and have observed changes in the BN spectrum. To minimize the operator error and enable future application of BN measurements in the hot-cell environment, specimen holder with sensor fixed under the sample was used. This report discuss the optimization of the measurements of recrystallized coarse-grained ODS steels, characterizes the key parameters of the measurements and consequently present the results of the investigation of thermally aged materials.

4. Results

4.1. PALS

4.1.1. PALS characterization of the studied materials

Analytical data processing was performed using the LT 9.0 program and two-component decomposition of the spectra. The lifetime spectra were fitted with a variance of fit (FV) ranging from 0.97 to 1.18 after source correction. As can be seen in Table 4.1.1, no presence of dislocations (or very small dislocation density respectively) has been observed in the recrystallized materials and the first lifetime component, which is then solely attributed to bulk annihilation, is reduced according to the standard trapping model [23]. On the other hand, the as-extruded ODS materials and reference Eurofer 97 show τ_1 values close to or higher than the bulk lifetime (108ps) and therefore τ_1 is considered to result from a combination of bulk annihilation and trapping in defects, here assumed to be dislocations. Their concentration can be consequently quantified according two defects model described by Vehanen et al [23]. Dislocation densities calculated for the studied materials are listed in Table 4.1.1.
In all ODS steels investigated, a longer component of ~240ps was found. Its value can be assigned to both yttria nanoparticles [24] and small clusters with the mean size of 4-5 vacancies[2] which are a result of mechanical alloying procedure [25, 26]. We assume that these defects are associated in particular with the yttrium and yttrium aluminium oxides where they have higher thermodynamic stability and a higher probability to "survive" the recrystallization. It is clear that positron trapping in small vacancy clusters and yttria particles in the ODS steels can hardly be distinguished experimentally. Reasonable estimates for the individual positron trapping processes can be made, however, using known characteristics of yttria nano-features (YNF) (see Table 2.2). Detailed calculation procedure proposed for the processing nano-structured materials PALS spectra, based on combination of diffusion and transition trapping regimes, can be found in [27].
As can be seen in the results from the above-described data processing (Table 4.1.1), positron trapping at YNF is reduced in the recrystallized materials. This effect can be attributed to decreasing of YNF concentrations, which accompany YNF coarsening at temperatures closely below the melting temperature.

Table 4.1.1 – PALS results, calculated densities of various defects and individual fractions of positrons annihilated in the material bulk and various defects (dislocations, vacancy clusters and yttria nano-features). MLT is the positron mean lifetime given as weighted average of two lifetime values

	PALS results					Defect concentration		Positron annihilation / trapping			
Material	τ_1 [ps]	τ_2 [ps]	I_2 [%]	MLT [ps]	FV	$N_{disl.}$ [m^{-2}]	$N_{VC\ (4V)}$ [m^{-3}]	Bulk [%]	Disl. [%]	VC [%]	NF [%]
PM2000 ex.	129	253	54	196	1.09	1.4×10^{14}	1.9×10^{23}	19	27	34	20
MA957 ex.	152	256	57	211	1.00	4.5×10^{14}	5.5×10^{23}	7	36	39	18
ODS EU ex.	127	245	51	187	1.18	1.2×10^{14}	1.0×10^{23}	22	28	20	30
MA956 rec.	87	252	54	176	1.03	-	8.5×10^{22}	55	-	33	12
PM2000 rec.	83	241	54	168	1.05	-	8.2×10^{22}	57	-	31	12
ODM751 rec.	85	260	48	169	1.11	-	6.0×10^{22}	62	-	25	13
Eurofer 97	99	202	42	142	1.00	2.4×10^{13}	1.6×10^{23}	58	11	31[3]	-

[2] In case of the reference Eurofer 97 material, the second lifetime component can be attributed to divacancies in Fe [28].
[3] Calculated for di-vacancies.

As can be seen from Figs. 4.1.1 and 4.1.2, the highest positron mean-lifetime caused by the highest fraction of positrons trapped in lattice imperfections (dislocations, vacancies, YNF) was observed for the MA957 material. Although this material has the lowest content of Y_2O_3, its oxide particles exhibit the finest dispersion structure reducing the distance between particles and increasing the probability of positron trapping. Actually, in this material positron trapping is close to saturation level (annihilation in bulk is only ~ 15%). On the other hand, the recrystallized materials with oxide particle sizes about 10 times higher show ~ 2 - 3 times lower positron trapping in YNF than the as-extruded materials.
It is important to note that the vacancy type defects should be considered in conjunction with the YNF. In fact, the presence of vacancy type defects seems to stabilize the oxide particles [29, 30], a hypothesis which, in principle, can by explored by PALS experiments. This issue, however, requires further research in order to elucidate the role of vacancies in the structural stability of YNF.

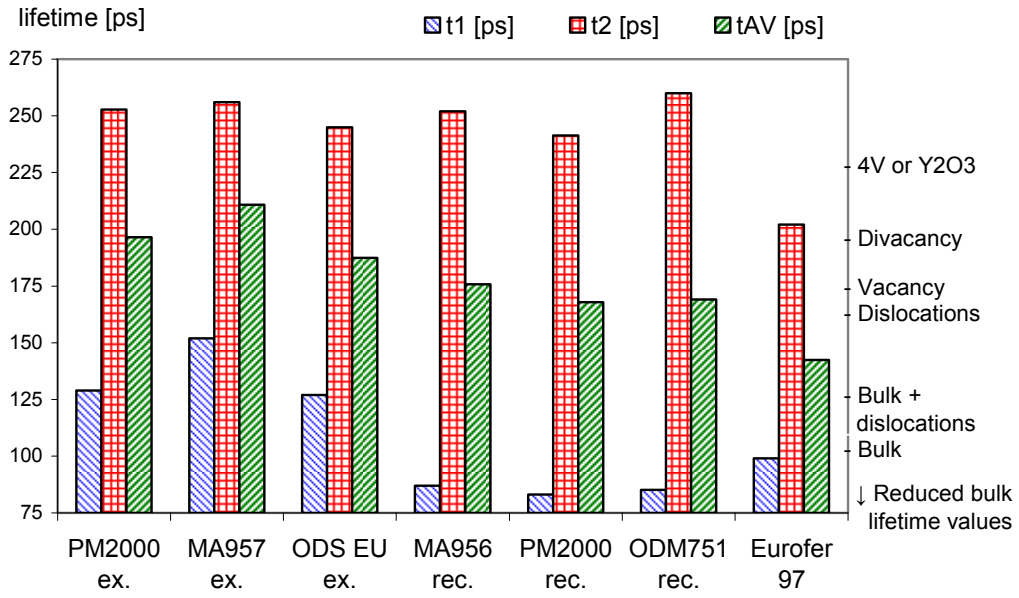

Fig. 4.1.1. Positron lifetimes in the investigated materials

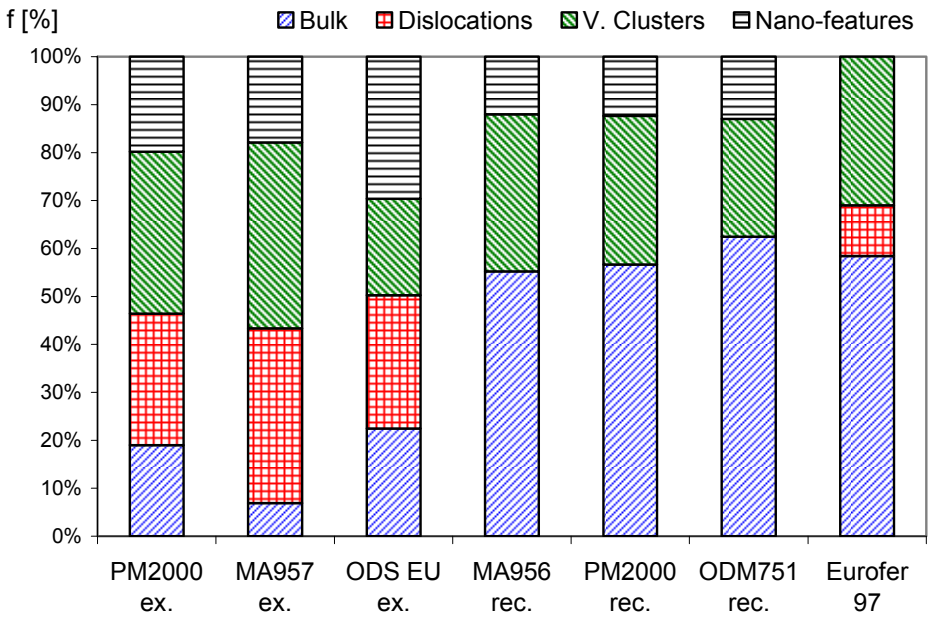

Fig. 4.1.2. Fractions of positron annihilations in bulk and individual trapping sites

Measurements of positron lifetimes in the ODS materials (three recrystallized ODS steels and the ODS Eurofer) aged at 475°C show the evolution of vacancy type defects with annealing time. The behaviour of the average positron lifetime $\tau_{AV} = \sum I_i.\tau_i$ (Fig. 4.1.3), which is considered to be the statistically most robust parameter, shows different trends for the individual materials. Since the coarsening of oxide particles below ~1100°C is negligible, we can attribute these changes to the mobility and recovery of vacancy type defects. As can be seen in the Fig. 4.1.3, three different behaviours have been observed. We assume that in case of PM2000 and ODM751, dissociation of vacancy clusters, which saturates after 100h and 500h respectively, is taking place [31]. MA956 does not show this phenomenon and in fact no significant changes were observed during the thermal treatment. In contrast to this, average positron lifetimes of ODS Eurofer increase after aging up to 500h. Similar behaviour was observed by Rajaraman et al. [31] for the Fe-Y_2O_3 steel thermally aged at intermediate temperatures.

When only one type of trapping centre is considered to determine the large component of the positron lifetime spectrum, the calculated concentrations of these centres for individual materials are 1 – 3.5×10^{23} [m^{-3}]. This would be in good agreement with the PALS experiments of Alinger et al. [25]. These trapping centres, however, cannot be considered neither as YNF nor as vacancy clusters, but rather as a combination of both. Since the information about the mean size and concentration of yttria nano-particles was available for the present materials, we have diffusion limited trapping model [27] to estimate fractions of positron trapping at these particles. Once, the trapping at YNF was determined, trapping at vacancy clusters (VC) was calculated as difference between experimentally measured trapping and the trapping at YNF (Table 4.1.1).

For the calculation using diffusion limited trapping we have used the diffusion length (40nm) adopted from the literature [32], experimentally obtained for iron-based model alloys with similar concentrations of vacancy type defects. Our experiments show that the value of 40nm is fairly close to the actual values of positron diffusion lengths for the materials investigated here, since the maximum possible value obtained from the experimentally measured trapping rate is $L_+ < 50$nm for as-extruded materials and $L_+ < 65$nm for recrystallized materials[4].

[4] For comparison, the positron diffusion lengths reported for defect-free metals is ~ 100nm [33].

Higher values would lead to trapping rates higher than the actually measured ones. In other words, longer diffusion lengths would imply the positron trapping to occur exclusively in the YNF and the presence of vacancy type defects, if any, would be associated to those particles only. This is however at variance with the observation that positron trapping at vacancy clusters was reported in mechanically alloyed materials without oxide nanoparticles as well [34]. So the presence of vacancy clusters seems to result from the fabrication process, rather than from the presence of nano-oxides.

4.1.2. PALS characterization of the 475°C embrittlement

The effect of α' precipitation, which is one of the key factors in the thermal (radiation) embrittlement of high Cr steels, cannot be observed in Fe matrix by positron lifetime technique directly. Positron lifetime of Cr bulk is very similar to Fe bulk, while the positron affinity of Cr is even lower than the one of Fe. This is the reason why the positron trapping at nano-sized Cr precipitates cannot be distinguished in the lifetime spectra. However, various studies published in the literature report effect of Cr rich zones on the mobility of vacancy clusters, which indicate a possibility of application of PALS technique on the study of the α' precipitation. In the paper by Kuramoto et al. [35] authors describe the effect of chromium precipitation on the formation of microvoids in the thermally annealed Fe-Cr alloys. This work concludes that the tendency to formation of microvoids is lower when Cr enriched zones are present in the matrix. The presence of such zones-precipitates was observed in our thermal aging experiments for high-Cr materials.

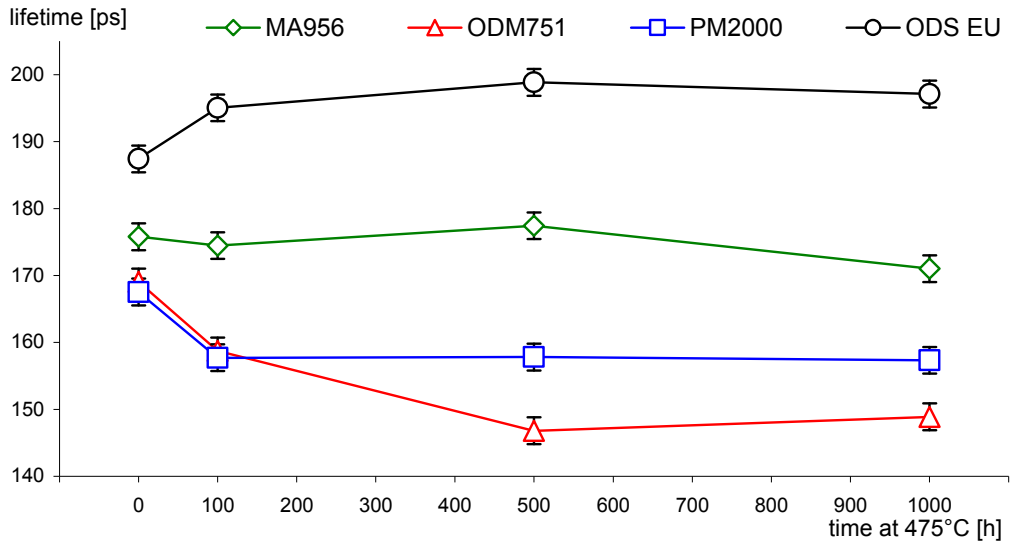

Fig. 4.1.3. Average positron lifetime in the isothermally aged materials.

Direct evidence for α' precipitation was obtained from the small angle neutron scattering, where new ~ 5 nm scattering centres appeared after 100h hours of thermal aging and indirect confirmation was provided also by microhardness measurements, results of which are shown in Fig. 4.1.4. Consequently, the measurements of positron lifetime showed that an agglomeration of vacancies took place only in the ODS Eurofer material, where the Cr-rich α' precipitation was not observed (Fig. 4.1.4). Accordingly, the fraction of positron trapping at vacancy clusters calculated from experimental results shows that this value increases with the time of the thermal aging for the ODS Eurofer in contrast with the PM2000 and ODM751 materials and early stages of the MA956 material (Fig. 4.1.5). We assume that this is due to the presence of Cr precipitates in the 16-20%Cr materials where the formation of vacancy agglomerates is hindered and consequently indirect PAS observation of this phenomenon is possible.

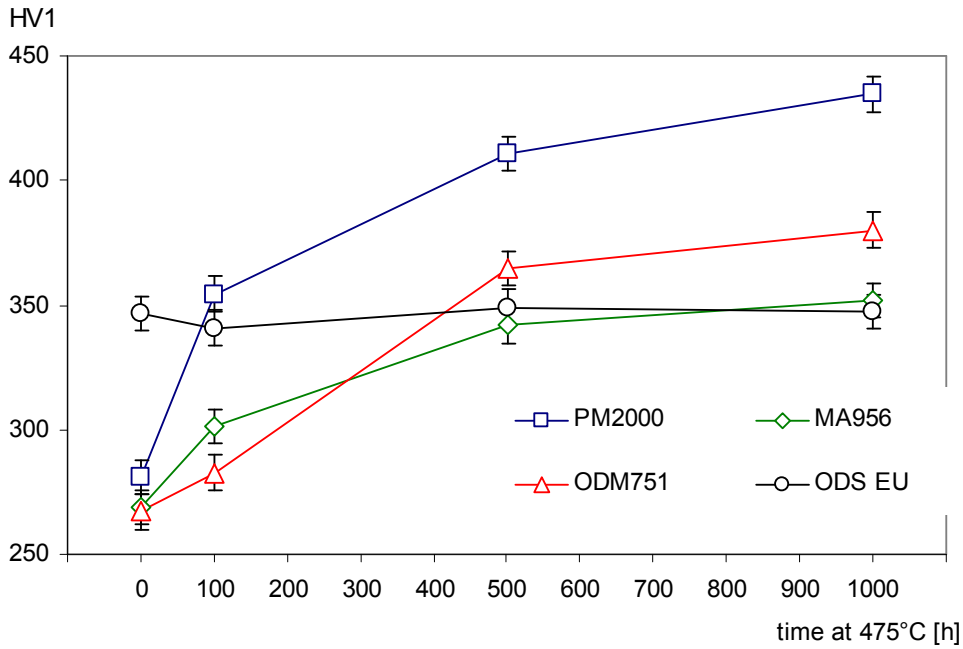

Fig. 4.1.4. HV1 results of the isothermally aged materials

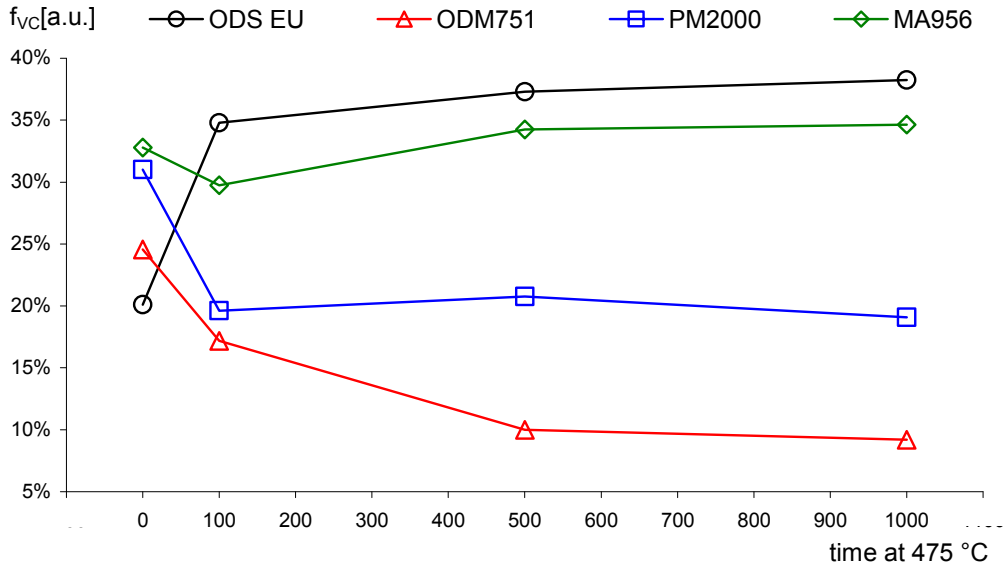

Fig. 4.1.5. Fraction of the positron trapping at vacancy clusters of the isothermally aged materials.

On the other hand, the work of Malerba et al. [36] concludes that although the presence of Cr in ferritic (ferritic/martensitic) alloys has an effect on radiation induced defects formation, the dependence of this effect on Cr concentration is non-monotonic and therefore difficult to rationalize. Yet it is not clear how the elevated temperature irradiation results can be extrapolated to the thermal-only degradation studies. Not only the role of chromium in material degradation, but also the effect of yttria nano-particles on the behaviour of the Fe-Cr systems needs further research to be carried out in conjunction with other techniques, providing complex information about all nano-sized features related to the process of radiation embrittlement.

4.2. SANS

The samples in the shape of plates 1 mm in thickness were measured at two detector positions 1.3 and 5.5 m and at wavelengths of 6.09 Å and 15.96 Å in BNC Budapest. The corresponding q range was from $4x10^{-2}$ nm^{-1} to 2.5 nm^{-1}. The samples were placed into external saturating magnetic field (~1.6 T) perpendicular to the incident neutron beam direction. The measured data were corrected for sample transmission, detector response and background. Data calibration was done using a water standard.

All materials showed a strong SANS signal in both the as-recrystallised and the aged states. The SANS measurements revealed that thermal treatments result in a substantial changes in the microstructure at the nanometer size scale. Fig. 4.2.1 shows the magnetic and nuclear coherent scattering cross-sections of the as-received and the three aged states of PM2000 material. The curves for MA956 have the same character. A pronounced ageing-induced increase is found on the magnetic and nuclear scattering curves at scattering vectors q>0.40 nm^{-1}.

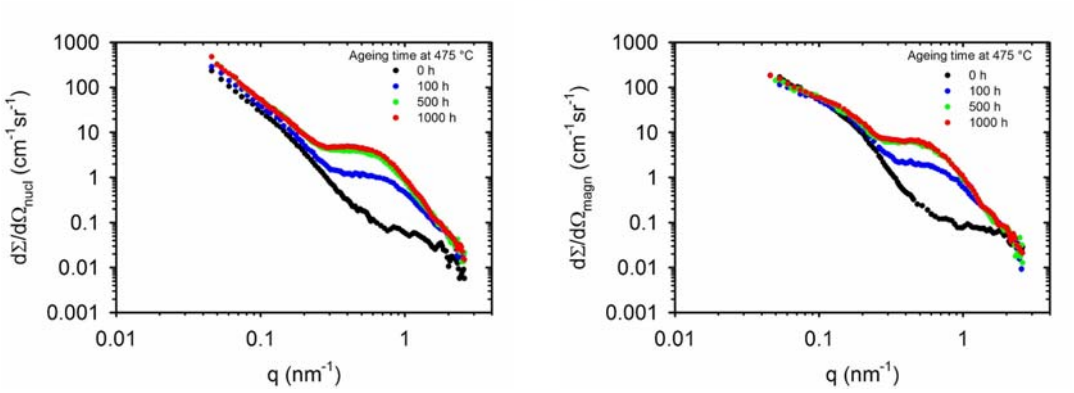

a) b)

Fig. 4.2.1. Nuclear and magnetic SANS scattering cross-sections for PM2000 in as-received and three aged conditions.

The aged material states were compared to the as-received material. We focused on the pronounced effects at q-values larger than 0.4 nm^{-1}, on the formation of small precipitates during ageing.

The analysis of the experimental results indicates formation of Cr-enriched precipitates (α' phase) at the nanometer scale during thermal ageing at 475 °C. From the SANS data the volume distribution functions for the different material states were calculated using the indirect transformation method developed by Glatter [37]. The corresponding size distributions are shown on Fig. 4.2.2.

The A-ratio (defined as ratio of the scattering cross-sections perpendicular and parallel to the magnetic field direction) of the aged MA956 samples (A=1.95±0.15) is in good agreement with α - α' phase separation of the ferritic matrix. Higher A-ratio (A=2.5±0.2) for PM2000 sample aged 100h indicates a mixture of α' particles and different type of scatterers.

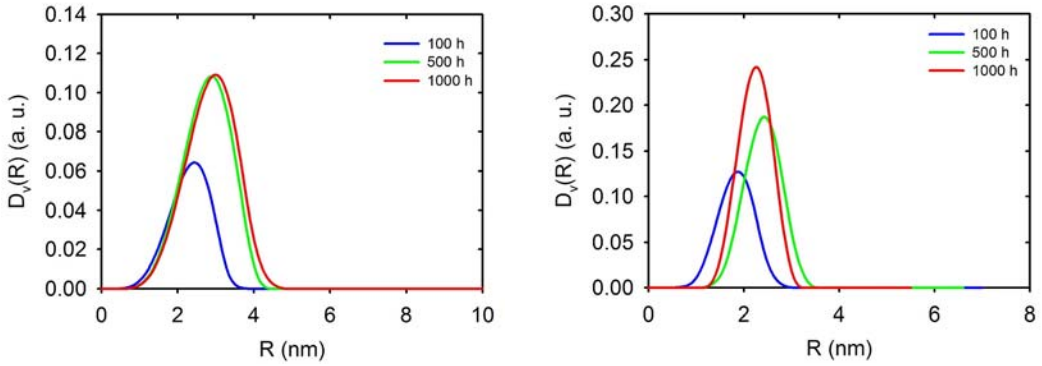

a) b)

Fig. 4.2.2. Particle size distribution at three aged conditions in PM2000 a) and MA956 b).

4.3. TEP

The Seebeck coefficient of the iron-based solid solutions depends strongly on the type and concentration of alloying elements. Although the Seebeck coefficient of iron against copper is +12.5μV/K [38], measurements on steels with copper[5] as the reference can result even in negative values. This is also the case of the investigated ferritic ODS steels where the Seebeck coefficient values were found to be in the in the range from -0.56 to -1.75 μV/K (Table 4.3.1).

Table 4.3.1 – Relative Seebeck coefficients of the as received ODS alloys measured with the copper as a reference material.

Material	PM2000	MA956	ODM751
S (μV/K)	-1.41	-1.75	-0.56

The ageing at 475 °C increased the relative Seebeck coefficient for all three materials. The dependence of the relative Seebeck coefficient on ageing time is shown on Fig. 4.3.1. The small-angle neutron scattering measurements (paragraph 4.2) showed that during ageing at 475 °C decomposition of the ferritic matrix into Cr-rich α' and Fe-rich α phases occurs. The increase of the relative Seebeck coefficient can be therefore directly related to the formation of the α' precipitates. There is a good correlation between the precipitated volume fraction and the increase in the S parameter (fig. 4.3.2).
As can be seen in the Fig. 4.3.3, the change of the Seebeck coefficient corresponds very well to the evolution of the hardness of the heat treated materials too. On the other hand, no increase of the Seebeck coefficient was observed for the materials aged at 650°C (Fig. 4.3.1 – dashed lines). At this temperature the matrix remains single phased, α.

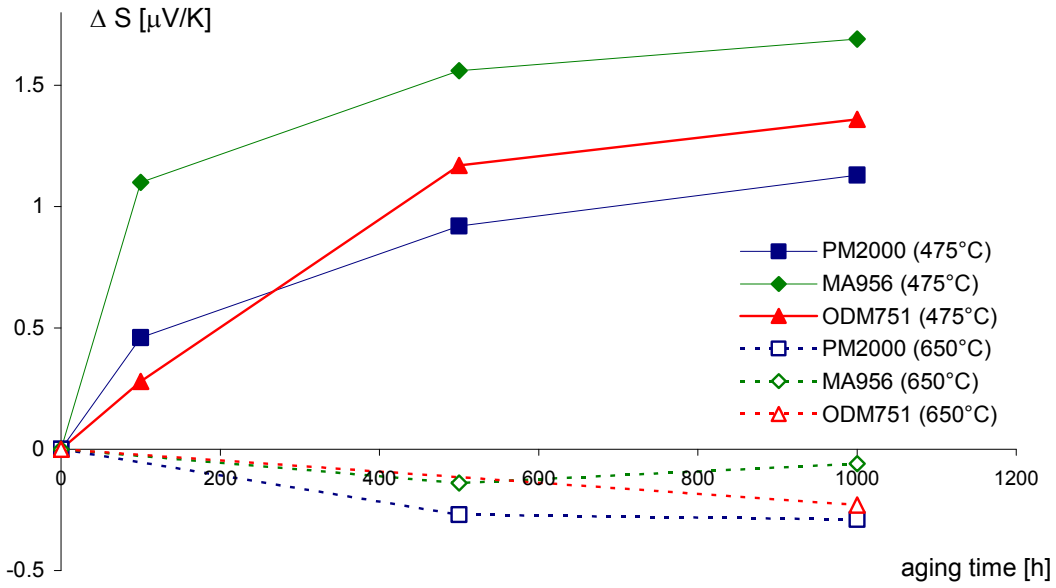

Fig. 4.3.1. Relative Seebeck coefficient of the thermally aged materials. Measurements with the copper reference.

[5] Hereinafter the thermoelectric power coefficient is always given as a relative Seebeck coefficient or ΔS measured against copper, unless stated otherwise.

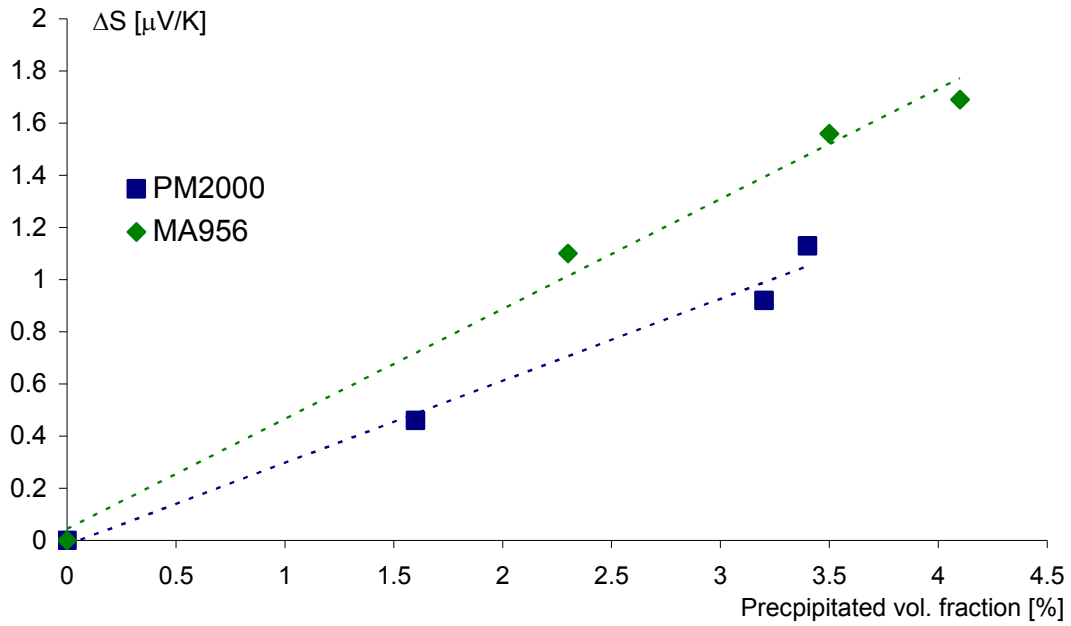

Fig. 4.3.2. Correlation of the Seebeck coefficient with the volume fraction of the precipitates.

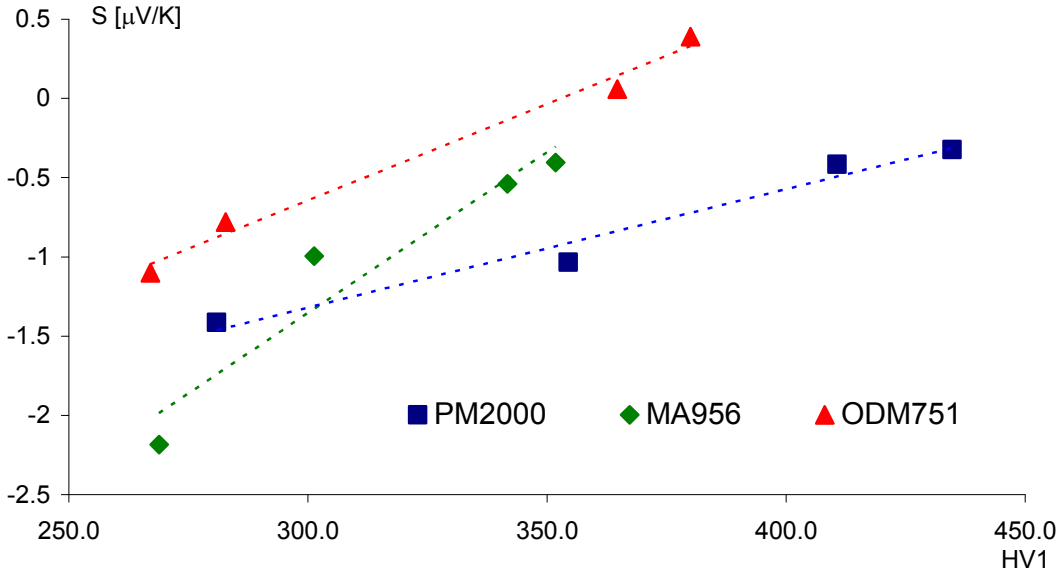

Fig. 4.3.2. Correlation of the Seebeck coefficient with the hardness measurements on the materials aged at 475°C for 0 - 1000h.

4.4. BN

The major challenge associated with the Barkhausen noise technique is that no commonly accepted standard for BN measurements has yet been established. This complicates the correlation of data between experiments and weakens the potential contribution of this technique to material research. In order to improve the reproducibility of the results as well as the understanding of the microstructural effects on the BN spectra of mechanically alloyed ODS steels, we proposed series of measurements. In these measurements we have investigated following effects:

The results of these measurements (see chapter 4.4.1 – 4.4.5) discuss the feasibility of the BN technique in the area of mechanically alloyed material. Based on these result, comparative measurements of various ODS has been performed. The results of these experiments are discussed in details in the chapter 4.4.6.
Finally, the Barkhausen noise experiments were performed on heat treated materials in order to investigate the 475°C embrittlement phenomenon. Chapter 4.4.7 discuses measurements of PM2000 and MA956 samples thermally aged at 475°C for 100, 500 and 1000 hours in order to study the hardening due to precipitation of Cr-rich phase. In the second part of this experiment, set of samples was aged for 500 and 1000 hours at 650°C in order to induce thermal changes in the microstructure without precipitation of chromium.

4.4.1. Experimental data processing

Experimental data in form of BN signals were recorded and digitally processed using the computer program μScan (supplied by Stresstech). This is preceded by the setting of measurements parameters, which are controlled by the same software. Following parameters are set:

1 Magnetizing frequency [Hz] – Frequency of magnetizing field (0.1 - 1000 Hz). This parameter determines the penetration (measurement) depth. The BN signal is attenuated by the eddy current opposition to an extent that depends on the frequency of the signal.
2 Magnetizing voltage [V] – Amplitude of magnetizing field applied to the specimen (0 - 20 V).
3 Magnetizing offset [V] – DC bias of the magnetizing field applied to the specimen.
4 No. of bursts – Number of half-periods of BN bursts that are stored and analyzed.
5 Sampling frequency – Rate of sampling of the signal for digital processing.
6 Signal input scale – Determines the maximum voltage of the analogue-digital (AD) conversion. The best resolution can be achieved when input scale is chosen so that the maximum value obtained from the measured samples are about 70-90% of the maximum values of the input scale.
7 Magnetizing current input – Displays the magnetizing current curve. This can be used to check the quality of magnetizing current in order to achieve undisturbed sine wave signal.
8 Magnetizing current input scale – Set the displayed magnetizing current scale.

After parameters setting is complete measurement can be processed. Following screen (Fig.4.4.1 left) displays the BN signal and enable operator to check/set the following characteristics:

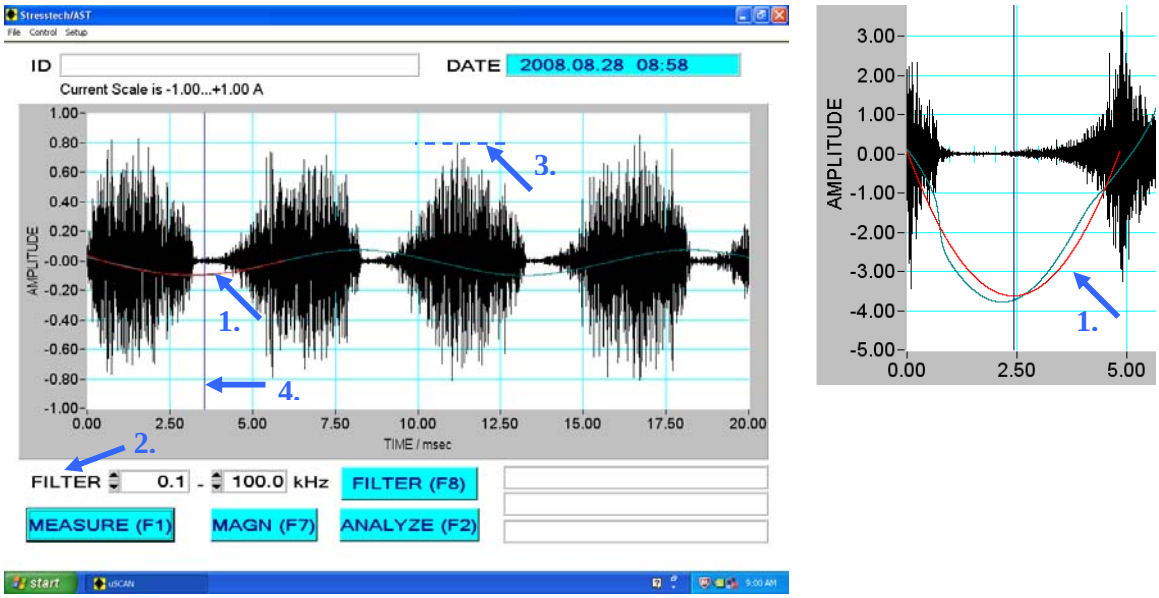

Fig. 4.4.1. Screen of the BN signal to be processed (left) and severe disturbance from the sine wave of magnetizing current (right).

1. Disturbance in sine form of magnetizing current. If the disturbance is significant (Fig. 4.4.1 right), operator should decrease magnetizing voltage.
2. Setting of band-pass filter.
3. Check if the major part (70-90%) of the burst is in selected input scale.
4. Setting of starting point for PEAKPOSITION evaluation. Default settings is at the magnetizing current minimum.

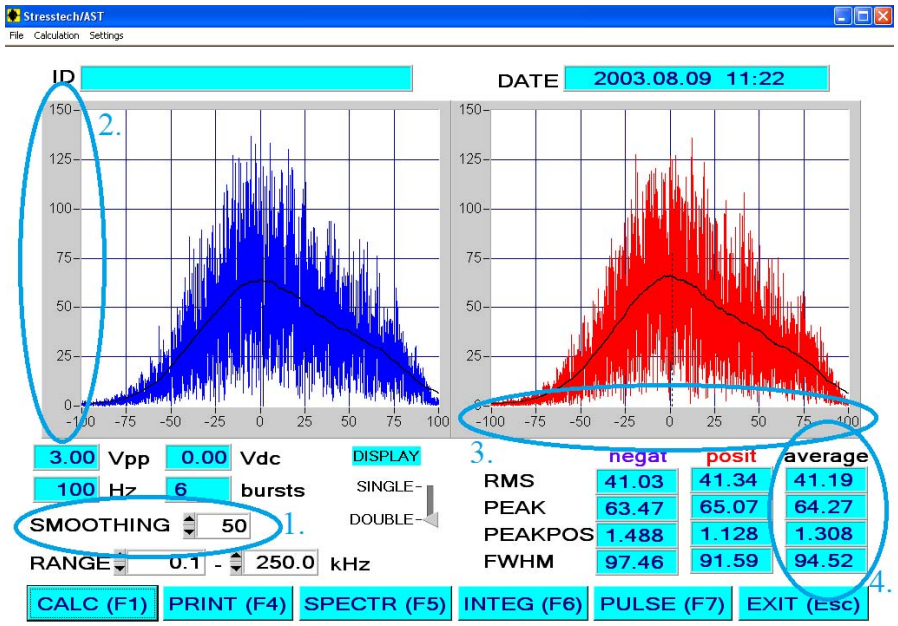

Fig. 4.4.2. Final screen with the characteristics of positive, negative and averaged signal.

Analyzed spectrum is displayed on the following screen (Fig. 4.4.2) and enable operator to review the following characteristics:

1. Smoothing of the signal envelope determines the accuracy of the processed curve. Higher values of this parameter increase the computing time.
2. Y-axis scale is set automatically. 100% corresponds to value set in signal input scale in the measurement settings window. Manual setting is possible via separate axis scale window.
3. X-axis scale represents percentage of the magnetizing current amplitude value (-100 correspond to magnetizing current minimum, +100 correspond to magnetizing current maximum).

This screen also provides final results in form of four calculated parameters:

1 RMS – Root mean square of all signal amplitudes sampled is given in percentage of the input voltage scale. RMS is not affected by smoothing parameter.

2 PEAK – The maximum value of the smoothened envelope curve. Result is given in percentage of the input voltage scale.

3 PEAKPOS – A parabola fits the 15% of the top of the envelope curve. The maximum of this parabola is the value of peak position. Result is given in percentage where -100 correspond to magnetizing field minimum and +100 correspond to magnetizing field maximum.

4 FWHM – Full width half maximum of the smoothened envelope curve of the rectified BN burst. Result is given in percentage difference of the magnetizing field in the left and right half-value of the curve.

4.4.2. Manual handling and alignment of the sensor

Commercial vendors of Barkhausen noise sensors provide a variety of sensors for different usage in the industry. Typical setup of the material inspection consists of sensor and a (rotating) sample holder. For the laboratory purposes at JRC-IET a general-purpose sensor is used (Fig. 4.4.3a). The application of this sensor, designed for investigation of medium and large surfaces, suffers with lower repeatability of the measurements of small samples (~10x10mm).

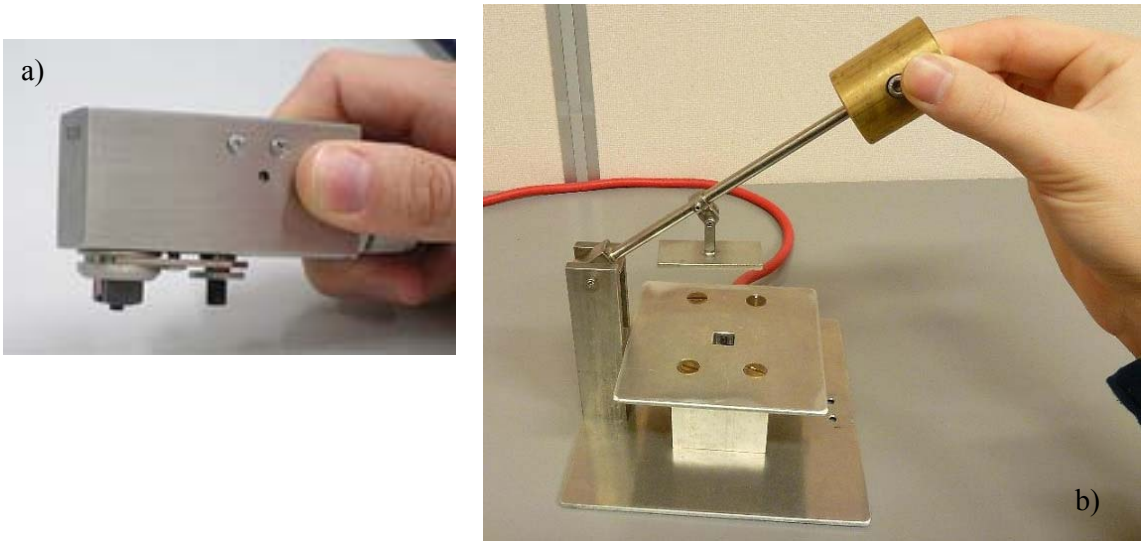

Fig. 4.4.3. General purpose sensor (a) and BN sample holder (b)

In order to improve the repeatability of measurements and minimize the effect of manual handling on the results, we designed a new sample holder with fixed sensor (Fig. 4.4.3b) and constant compressive force (8N). Design of the holder enables to measure samples as thin as 0.5mm with surface area < 100mm^2 with very good repeatability of the results.

4.4.3. Orientation of the sensor with respect to grain boundary

One of the major challenges in the BN study of the recrystallized ODS materials is the anisotropy of the microstructure with large grains. In the first approach these grain boundaries can be characterized as concentration centres of pining sites for magnetic domain movement. It is therefore reasonable to expect sensor position with respect to grain boundaries to have an effect on the Barkhausen noise signal. In order to better understand this effect, series of measurements has been performed on the recrystallized PM2000 sample cut perpendicular to the extrusion direction. The position of the sensor in the measurements and the corresponding BN signal envelopes can be seen in the Fig. 4.4.4. Set parameters for the BN measurements are shown in the Table 4.4.1.

Table 4.4.1 – Set parameters for BN measurements

Magnetizing frequency	40 [Hz]
Magnetizing voltage	10 [V]
Number of bursts	6
Sampling frequency	5 Mhz
Band-pass filter	0 – 200 [kHz]
Signal amplifying	x10
Smoothening	70

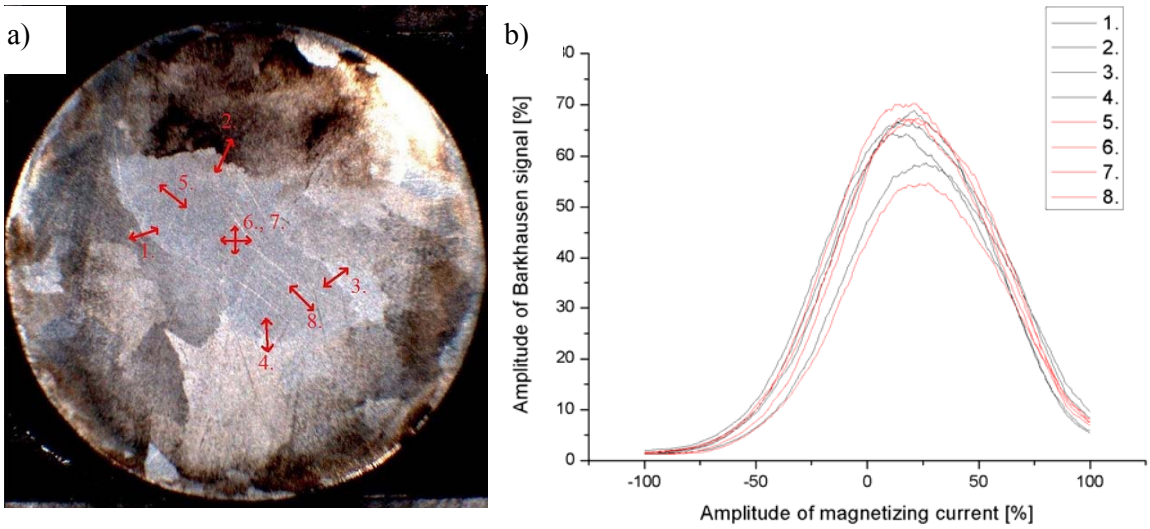

Fig. 4.4.4. Positions of the pick-up coil with respect to the grain boundary (a) and results of the BN measurements (b)

As can be seen from the Fig. 4.4.4b, the amplitude of the signal does not show any systematic difference between cases when the sensor was placed in grain or on the grain boundary respectively. Similar results were reported in [39]. As can be seen in the Table 4.4.2, the values of individual BN signal parameters are rather scattered. On the other hand, the average values of these parameters for measurements in the grain and on the grain boundary are comparable. Therefore, no particular conclusion can be made on the effect of the grain boundary on the Barkhausen noise signal in the investigation of coarse grained mechanically alloyed materials.

Table 4.4.2 – BN signal parameters of the PM2000 material, measured with different sensor position

PM2000	Position	RMS	PEAK	Peak Position	FWHM
Grain boundary	1	41.05	66.36	14.38	80.90
	2	33.86	55.22	19.40	79.87
	3	41.51	67.06	17.14	82.63
	4	43.67	70.19	13.19	83.64
Average		**40.02**	**64.71**	**16.03**	**81.76**
Grain interior	5	37.11	60.65	18.40	80.69
	6	42.90	66.34	13.03	90.87
	7	39.40	64.23	11.90	80.90
	8	41.84	68.45	14.82	78.72
Average		**40.31**	**64.92**	**14.54**	**82.80**

4.4.4. Effect of the size of sample

Our previous experiments on Barkhausen noise confirmed that it is difficult to compare the results obtained on a different size of the measured samples. Particularly the signal RMS and FWHM values significantly change with the different sample size. These changes obviously depend on the used parameters of the magnetizing field and must be considered in the spectra interpretation. In order to better understand the effect of sample size on the results of BN measurements a series of measurements with two different sample designs of the same material (PM2000 as-recrystallized) were performed. First sample (further referred as "thick") was 20 mm long rod with $\phi = 25$ mm. The second sample (further referred as "thin") was 1 mm thick plate cut from the same rod. Both samples were cut perpendicular to the extrusion direction of the rod. In all measurements the magnetic field was oriented parallel to their cut surface. Since the damping of the magnetization of sample is a function of frequency and it might be an object of concern in this experiment, we have used three different frequencies for our measurements. The calculated penetration depths as well as other setting used can be seen in the Table 4.4.3. Based on the expression for eddy current density changes in a semi-infinite conductor (see below), maximum penetration depth 3.1mm was calculated for the frequency 100 Hz. Lower frequencies were not used due to worse repeatability of the measurements (see chapter 4.4.4).

$$\delta = \frac{1}{\sqrt{\pi f \mu \sigma_e}}$$

Where:
δ = standard depth of penetration (mm)
f = magnetizing frequency (Hz)
$\mu = 200$ = relative magnetic permeability of magnetic steel
$\sigma_e = 1.32$ [% IACS] = Electrical Conductivity of PM2000

Table 4.4.3 – Set parameters for BN measurements

Frequency [Hz]	100	150	200
Penetration depth of the magnetization [mm]	3.1	2.5	2.2
Magnetizing voltage [A]		3	
Band-pass filter [kHz]		0 – 200	

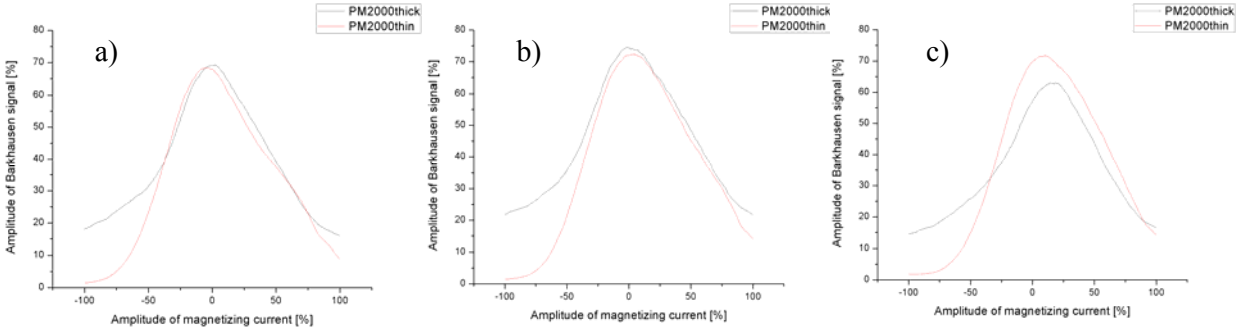

Fig. 4.4.5. BN signals measured for two different sample designs with magnetizing frequency 100Hz (a), 150Hz (b) and 200Hz (c)

As can be seen in the Fig. 4.4.5, BN signal envelopes differ between small and large sample volume of the measured sample. While in the thin sample the signal drops almost to zero values between bursts, signal from the thick sample remains at certain (background) level. We assume that this can be attributed to the volume of the ferromagnetic material from which the signal is received. While the magnetic domain walls movement in small sample is induced almost exclusively by external magnetic field, the signal from large sample is affected by complex wall interactions. These interactions can be observed as the noise between the signal peaks (Fig. 4.4.6).

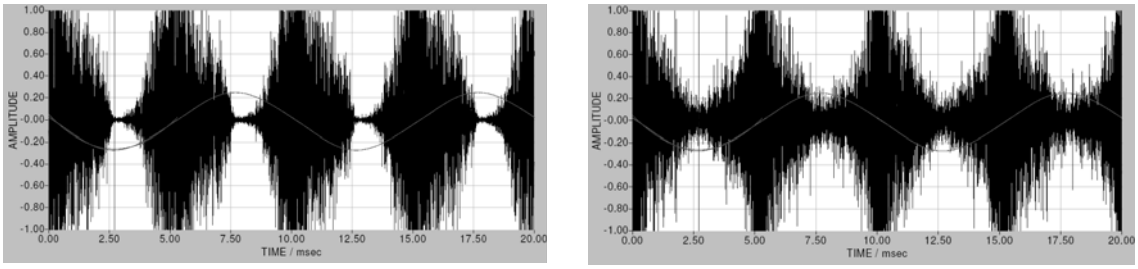

Fig. 4.4.6. Barkhausen noise power spectrum measured for small (a) and large sample (b) with the magnetizing frequency of 100Hz.

Individual BN frequency spectra shown in Fig. 4.4.7 do not indicate any systematic changes between the measured samples, which is in agreement with the expectations.

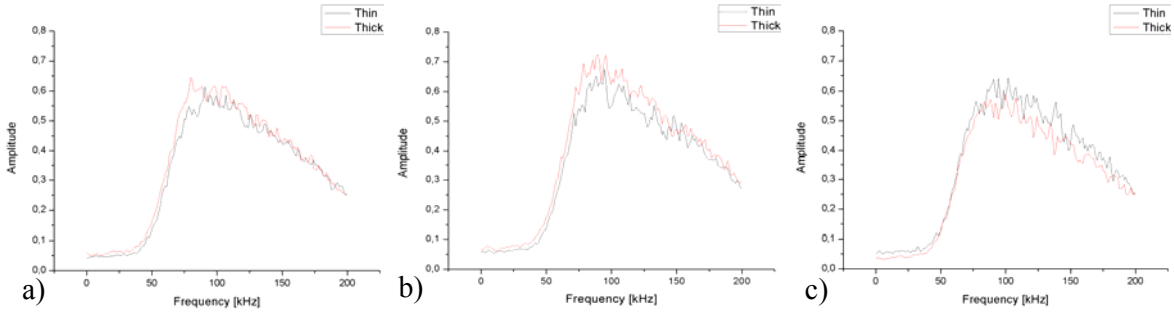

Fig. 4.4.7. Barkhausen noise frequency spectrum measured for two different sample designs with magnetizing frequency 100Hz (a), 150Hz (b) and 200Hz (c)

In general we can describe the effect of the sample dimensions/design on the Barkhausen noise signal as inessential, but it becomes important when RMS and FWHM values are taken into consideration. Small samples, where the dimensions are comparable with the eddy current penetration depth, result in smaller RMS values and larger FWHM values of the BN signal. This can be seen in the Table 4.4.4, where averaged results from 5 measurements are shown. Standard deviation σ is calculated for all four parameters considered.

Table 4.4.4 – BN signal parameters of the studied PM2000 samples

PM2000	F [Hz]	RMS	σ	Peak	σ	Peak position	σ	FWHM	σ
Thin	100	43.92	0.23	68.08	0.50	-3.41	0.89	94.90	2.45
	150	47.29	0.19	72.37	0.56	-0.26	1.11	95.84	1.20
	200	46.61	0.20	71.54	0.62	6.36	0.79	93.50	1.24
Thick	100	46.64	0.28	68.60	0.92	0.55	1.05	78.53	1.86
	150	51.73	0.46	74.13	1.36	-1.85	1.14	82.76	1.85
	200	41.85	0.41	62.73	1.20	11.18	0.78	75.48	2.77

4.4.5. Magnetizing frequency

Although many scientific publications report Barkhausen noise experiments performed with low frequency (3 - 10Hz) of the external magnetic field [39 - 41], our experiments on ODS materials with such frequencies did not resulted in a good reproducibility. As can be seen in the Fig. 4.4.8a the shape of the BN signal is strongly frequency dependent at low frequencies (10-70Hz). In the range 100-150Hz the envelope of BN signal is almost independent on the frequency (Fig.4.4.8b). With increasing frequency of the magnetizing field (>300Hz) BN signal is deformed and its parameters became again strongly frequency dependant.

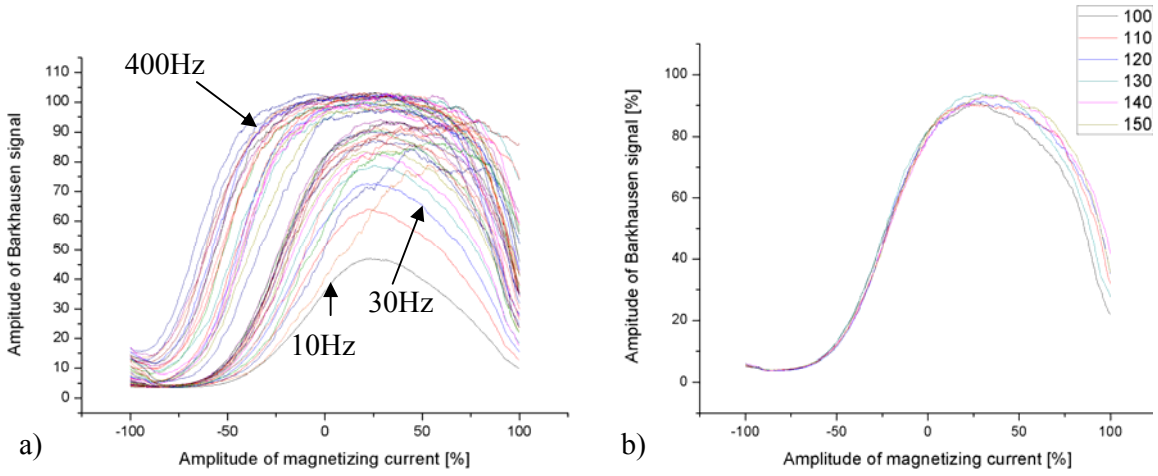

Fig. 4.4.8. Barkhausen noise signal as a function of the frequency of magnetizing field. Frequency 10 - 400Hz (a) and 100-150 Hz (b). Magnetizing voltage (1-20V) was adjusted in order to compensate frequency dependent BN signal amplitude (See Fig. 4.4.9).

From the frequency graph of the RMS and Peak position values can be seen that an optimal frequency range for Fig. 4.4.9 lies between 100 and 150Hz. In this range the signal is stable and independent on the magnetizing frequency. Based on this result and the results described in 4.4.3, we proposed the following measurements to be performed with the frequency of 100Hz.

As can be further seen in the Fig. 4.4.9, to achieve a reasonable signal output, usually it is necessary to correct the magnetizing voltage. Increasing of this parameter leads to increasing of the signal amplitude and shifting of the peak position to lower values.

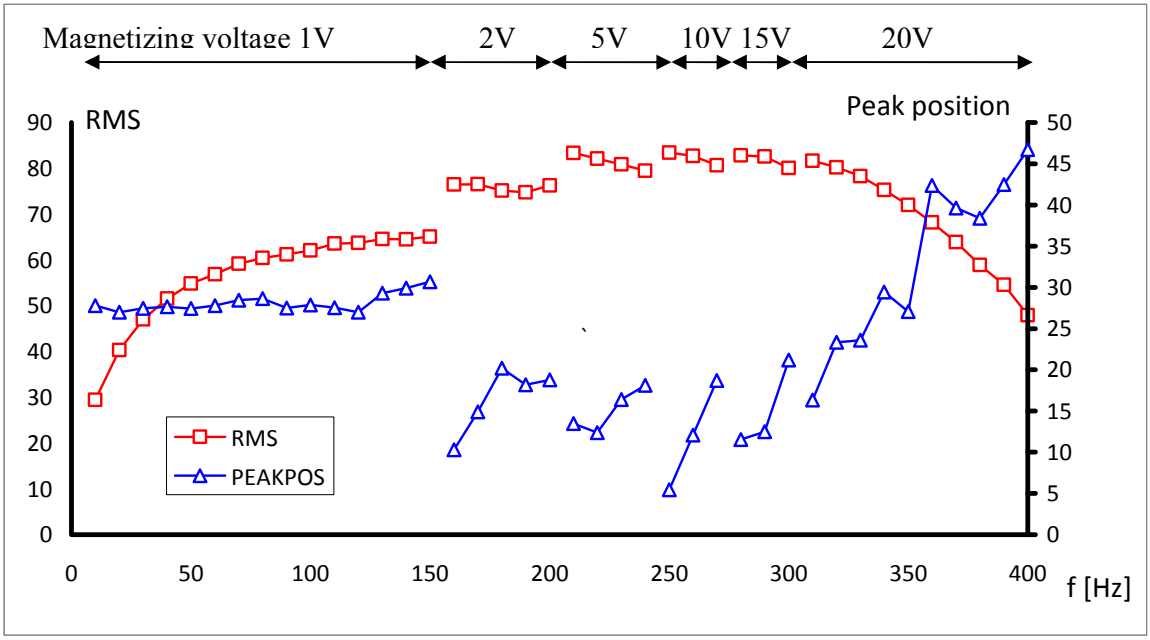

Fig. 4.4.9. RMS and Peak position values as a function of magnetizing field frequency.

4.4.6. Orientation of the magnetic field with respect to grain elongation

In all experiments described above the magnetic field was oriented perpendicular to the extrusion direction and the anisotropic (directional) properties of the materials were not discussed. It is, however, reasonable to expect that different mechanical properties, given by directional orientation of the grain structure, are reflected also in the changes of micro-magnetic properties. In order to investigate the influence of grain orientation on the Barkhausen noise parameters we have conducted series of measurements on the recrystallized PM2000, MA956 and ODM751 samples as well as on the as-extruded PM2000 sample. All samples were cut in the longitudinal direction and investigated with the external magnetic field oriented perpendicular and parallel to the grain elongation (extrusion) direction. Average values of individual BN signal parameters are listed in Table 4.4.5 and averaged envelopes obtained from 5 measurements in each direction are shown in the Fig. 4.4.10. Standard deviation σ is calculated for all four parameters considered.

Table 4.4.5 – BN signal parameters measured in perpendicular and parallel direction with respect to the grains elongation

	mag. field orientation	RMS	σ	Peak	σ	Peak position	σ	FWHM	σ
PM2000 recrystallized	parallel	38.51	0.43	56.65	0.79	9.17	1.03	108.36	1.78
	perpendicular	39.10	0.39	51.51	0.97	8.94	2.55	128.87	1.97
MA956 recrystallized	parallel	44.99	0.62	66.65	1.56	10.65	0.85	101.99	1.05
	perpendicular	51.21	0.39	73.59	0.49	4.09	0.47	109.97	0.87
PM2000 as-extruded	parallel	41.77	0.37	76.46	1.11	16.48	0.20	61.53	1.09
	perpendicular	45.92	0.23	80.05	0.58	14.97	0.80	69.86	0.74
ODM751 recrystallized	parallel	57.73	0.63	86.82	0.59	6.71	1.20	97.63	1.56
	perpendicular	51.76	0.95	79.79	2.30	14.62	0.77	94.38	1.50

As can be seen in the results, ODM751 material shows different behaviour than other three materials. While the MA956 and both samples of PM2000 show higher values of RMS and FWHM and smaller shift of the peak position for perpendicular directions, ODM751 acts the opposite way. We assume that this is due to different form of fabrication/product. While the

first three materials were supplied in the form of rods/sheets, ODM751 was supplied in the form of tube. Metal piping process creates strong residual stresses in the radial direction. We assume that these residual stresses are in the case of ODM751 tube higher than the axial residual stress and determine the directional characteristics of Barkhausen noise signal.

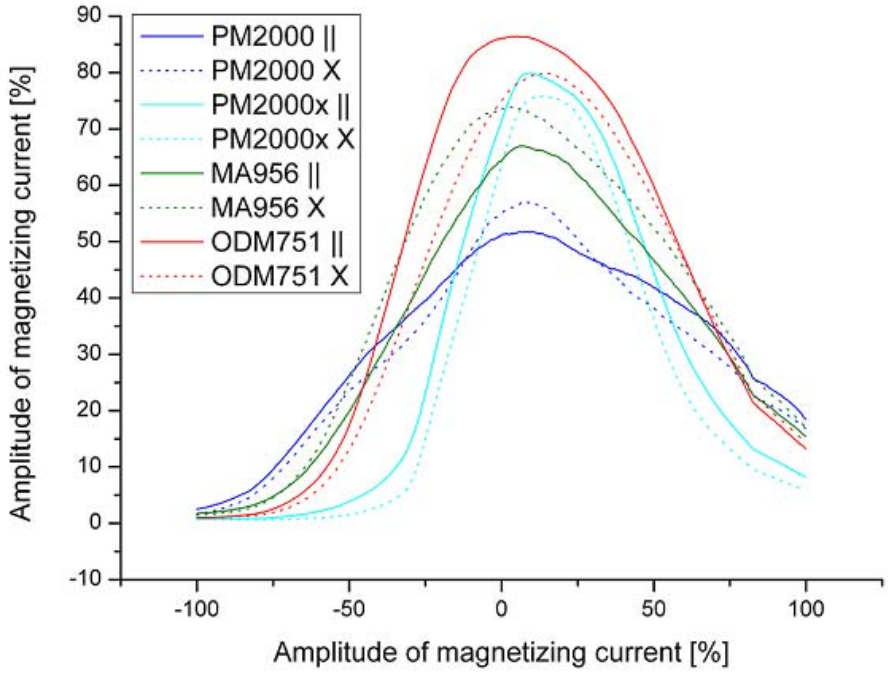

Fig. 4.4.10. Barkhausen noise signal envelopes (longitudinal cut samples).

4.4.7. BN characterization of the studied materials

Although the industrial application of magnetic Barkhausen noise technique is usually based on changes in the RMS parameter, in a complex material characterization based on the BN technique it is necessary to consider also the qualitative parameters of the signal, such as peak position and FWHM as well as frequency spectra of the noise. As it was outlined in the previous chapters, these parameters might be used as an indicator of concentration and distribution of microstructural defects. In order to verify these assumptions and contribute to the characterization of ODS materials, comparative measurements of various ODS materials were performed.

PM2000, MA956, ODM751, ODS EUROFER as well as conventional EUROFER97 were investigated in form of 10x10x0.5mm samples. In the case of MA957 material, 8x8x0.5mm sample was used. Based on the previous experiments, we used 100Hz magnetizing field for the comparative BN characterization of different ODS materials. In all measurements discussed in this chapter external magnetic field was oriented perpendicular to the grain elongation of the materials. Detailed experimental parameters settings are listed in the Table 4.4.6. The averaged results of the BN signal parameters from at least five measurements are listed in the Table 4.4.7. The averaged signal envelopes are shown in the Fig. 4.4.11.

Table 4.4.6 – Set parameters for BN measurements

Frequency [Hz]	100
Magnetizing voltage [V]	3
Number of bursts	6
Sampling frequency	5 Mhz
Band-pass filter	0 – 200 [kHz]

Table 4.4.7 - BN signal parameters of the measured materials

	RMS	σ	Peak	σ	Peak position	σ	FWHM	σ
PM2000 rec.	57.65	3.94	78.45	3.30	4.43	0.70	127.05	25.34
MA956 rec.	51.60	0.47	73.54	0.54	6.57	0.87	112.38	1.18
ODM 751 rec.	51.76	0.95	79.79	2.30	14.62	0.77	94.38	1.50
PM2000 extr.	41.77	0.37	76.46	1.11	16.48	0.20	61.53	1.09
MA957 extr.	18.10	3.16	29.65	6.90	27.00	2.53	80.32	11.01
ODS EUROFER	43.12	0.57	79.46	1.40	31.76	0.21	52.92	15.71
EUROFER 97*	53.79	0.50	83.60	1.06	15.50	0.86	92.87	1.31

* Conventional Eurofer 97 was measured as a reference material

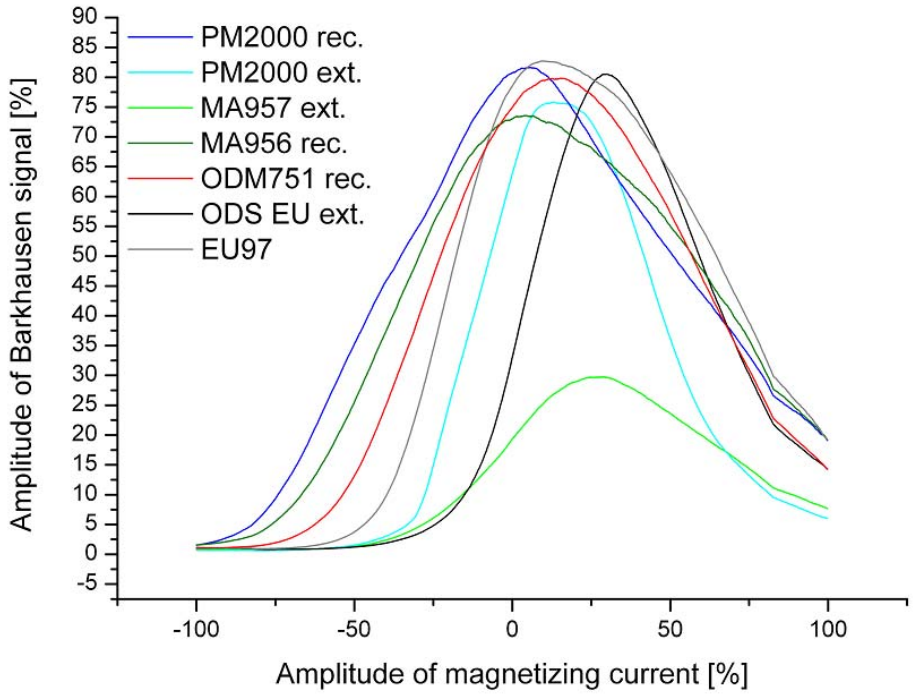

Fig. 4.4.11. BN noise signal envelopes measured for different ODS materials and Eurofer 97.

As can be seen in the Fig. 4.4.11, there is no clear difference in peak height and RMS values between as-extruded and recrystallized materials. Lower BN signal from the MA957 material can be attributed to the size of the sample, which was 8x8x0.5 mm (against 10x10x0.5 mm in all other materials). On the other hand, the FWHM and peak position seem to be dependent on the concentration of microstructural imperfections given by chemical composition and temperature history. As can be seen in the Fig. 4.4.12, smaller shift of the BN signal has been measured in recrystallized materials, with relatively low dislocation density and lower concentration of oxide particles. The most significant peak shift was measured for as-extruded materials with high concentration of yttria nano-particles. The pinning of magnetic domain walls is stronger in these materials, which results in delay of the Barkhausen noise response [42].

In the paper by Moorthy et al [43] authors discuss two groups of defects in the ER36 gear steel observed in Barkhausen noise measurements. First group of defects – weaker obstacles can be well investigated with a wide frequency spectrum of magnetizing field (4 - 125Hz). Here belongs for instance boundary of ferrite grain. Second group of defects, like carbides are considered as stronger obstacles and they can be observed only in the BN spectra induced by

lower frequencies of magnetizing field. It is assumed that lower frequencies lead to less significant eddy current opposition and therefore to a stronger magnetization. Experiments of Moorthy et al. with sufficiently strong effective magnetizing field (induced by frequency of 4Hz) result in an additional peak in BN spectrum, which is shifted to higher magnetizing field values. In other words we can say that the resulting BN spectrum, characterized by more than one peak is induced by more than one kind of domain wall obstacles. Consequently we can conclude that a larger spectrum of obstacles/defects leads to a wider BN signal, characterized by higher FWHM values. As can be seen in the Table 4.4.7, materials studied in our experiments exhibit different values of FWHM ranging from 52 to 127% of half-period of magnetizing field. In addition to this, peaks of the BN signal with higher FWHM (recrystallized materials) are shifted to the smaller values and vice versa (Fig. 4.4.13). This indicates the recrystallized materials to contain a larger spectrum of weaker obstacles, while as-extruded materials to contain smaller spectrum of rather strong obstacles. As one of the strong non-magnetic obstacles for domain wall movement, considered in the studied materials, is yttrium (yttrium aluminium) oxide, we assume that its characteristics determine the shift and width of BN signal. Consequently we can conclude that a rather wide range of coarsened oxide particles in the recrystallized materials act as weaker obstacles for magnetic domain wall movement and results in wider BN signal with relatively small shift of the peak. On the other hand, high concentration of fine oxide particles, characterizing as-extruded ODS materials, pin the domain walls stronger and the result BN signal is narrower and shifted to the higher values of magnetizing field.

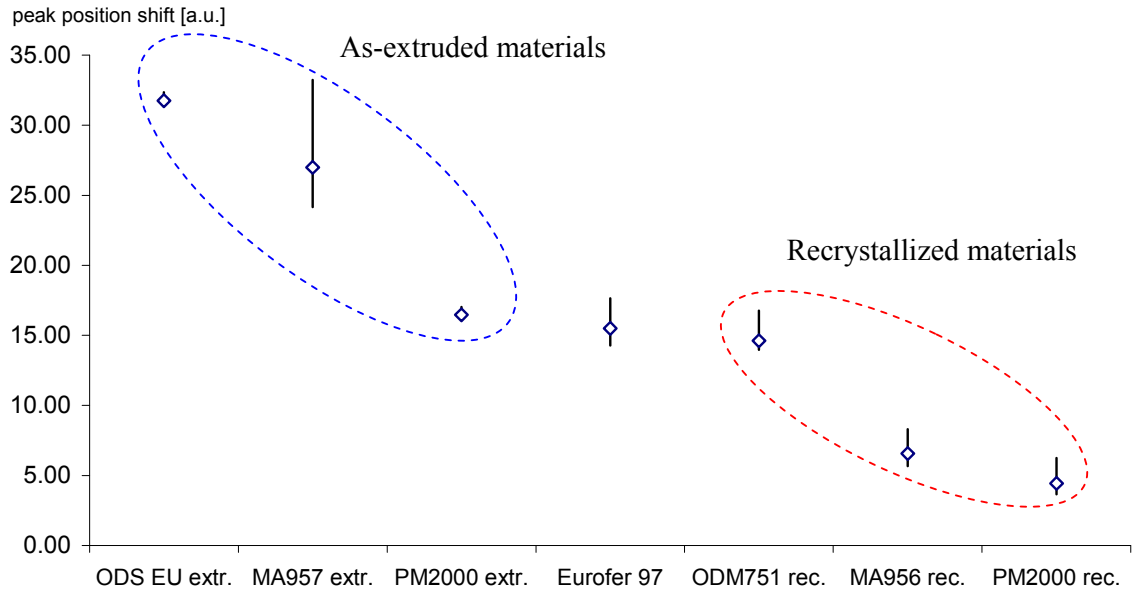

Fig. 4.4.12. Shift of the BN signal peak measured in various ODS and reference Eurofer 97 steel.

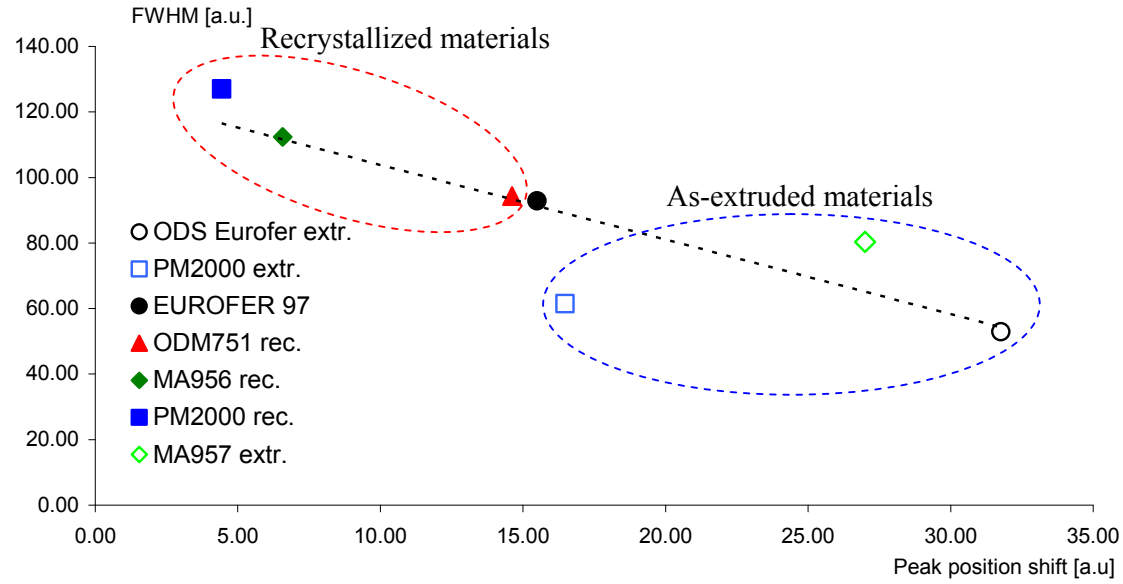

Fig. 4.4.13. FWHM value of the BN peak plotted as a function of the position of the peak.

Although the oxide particles in the studied materials seem to be important pinning sites for domain wall movement, their diversity does not affect BN frequency spectrum significantly. Fig. 4.4.14 shows frequency spectra of all investigated materials. All materials are characterized with BN noise frequency 50 – 200 kHz. Although the amplitudes of noise spectra differ between materials (Fig. 4.4.14a), the course of the frequency spectra is similar for all materials (Fig. 4.4.14b).

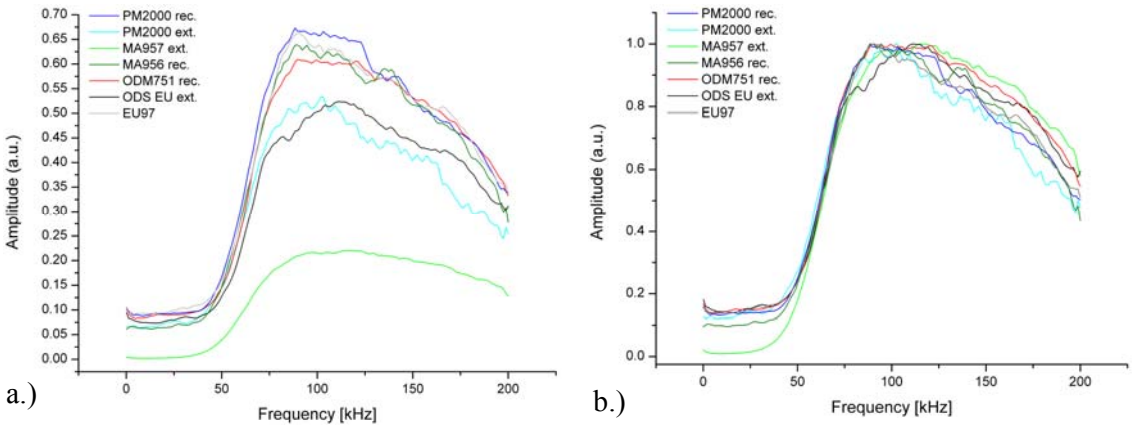

Fig. 4.4.14. BN noise frequency spectra of the measured materials smoothened (a.) and smoothened + normalized (b.)

4.4.8. BN characterization of the 475°C embrittlement

Series of Barkhausen noise measurements on the materials aged at 475°C were conducted. In order to distinguish in the measured parameters between the effect of precipitation of α' and the thermal annealing of the lattice, analogical thermal aging at 650°C was performed. Based on the previous obtained results and assuming the α' precipitates to be pinning sites for magnetic domain walls movement, we have investigated the position of the BN peak for different aging times of recrystallized PM2000 and MA956 materials (Fig. 4.4.15). The experimental results in the form of individual BN signal parameters are listed in the Table 4.4.8.

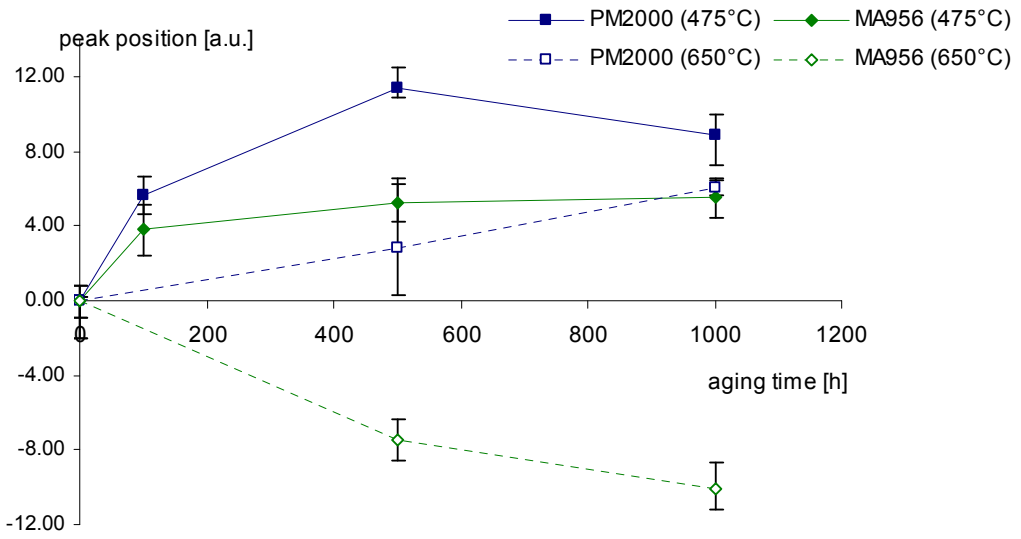

Fig. 4.4.15. Position of the BN peak obtained from heat treated PM2000 and MA956 materials.

As can be seen in the Fig. 4.4.15, both materials show different behaviour for 475°C and 650°C aging. While the 650°C thermal treatment leads to only relatively small increase of BN signal shift in PM2000 and significant decrease in MA956, 475°C aging significantly increases the shift of both materials. We assume that the shift of the BN signal to higher magnetizing field values is due to precipitation of new phase, which acts as stronger obstacle for domain wall movement. This assumption is in agreement with Moorthy et al. who observed second phase precipitates in Cr-Mo ferritic steel at higher field strength only [43].

Table 4.4.8 – BN signal parameters of the thermally aged materials

	Temperature [°C]	Time [h]	RMS	σ	Peak	σ	Peak position	σ	FWHM	σ
PM2000	As-received	-	57.65	3.94	78.45	3.30	4.43	0.70	127.05	25.34
	475	100	47.88	0.28	60.16	0.46	10.03	1.42	139.95	1.44
		500	43.52	0.30	59.63	0.52	15.84	0.89	119.59	1.32
		1000	52.78	0.14	69.81	0.36	13.32	1.47	129.57	0.27
	650	500	52.55	0.37	75.85	1.46	7.24	2.76	116.83	6.06
		1000	51.98	0.10	76.47	0.06	10.47	0.44	112.20	0.67
MA956	As-received	-	51.60	0.47	73.54	0.54	6.57	0.87	112.38	1.18
	475	100	49.33	0.53	70.99	1.16	10.43	1.35	110.20	0.95
		500	52.41	0.41	76.18	0.49	11.81	1.17	108.84	0.99
		1000	57.49	0.26	79.16	0.78	12.11	1.01	118.55	0.76
	650	500	54.83	0.20	76.62	1.21	-0.94	0.78	116.79	2.01
		1000	55.44	0.34	77.73	1.10	-3.49	1.03	117.40	1.07

5 Conclusions

This study describes the behaviour of the microstructure of the oxide dispersion strengthened steels at intermediate temperature. Four, in principle, different techniques were used for the characterization of the microstructure of the oxide dispersion strengthened steels thermally aged at 475°C. All techniques, namely positron annihilation lifetime spectroscopy, small angle neutron spectroscopy, thermoelectric power and Barkhausen noise measurements are very sensitive to metallurgical modifications and presence of nano-sized imperfections in the crystal lattice. As can be seen in the results, precipitation of the nano-sized α' phases, directly observed by SANS, affects the mobility of vacancy type defects, change the thermoelectric Seebeck coefficient of the high-Cr materials (PM2000, MA956 and ODM751) and shift the Barkhausen noise signal. Since previous TEM and XRD investigations did not confirmed other metallurgical changes in the materials, we assumed that the observed changes were mostly due to α' precipitation. The main conclusions obtained from the experiments are summarized bellow:

- Although the positron lifetime technique is not directly sensitive to the Cr-rich α' phase in the Fe lattice, the experiments showed that these precipitates affect the mobility of point defects and consequently change the annihilation characteristics.
- Presence of chromium rich zones in the ferritic materials with high Cr content (>15 wt%) plays a role in the mobility of point defects at 475°C. While in high-Cr alloys the thermal aging leads to annealing of vacancy type defects, Fe-9%Cr ODS Eurofer showed notable coarsening of the vacancy clusters. This may lead to a significantly different radiation performance of the low and high chromium alloys at intermediate temperatures.
- The SANS analysis indicated formation of Cr-enriched precipitates (α' phase) at the nano-meter scale during thermal ageing at 475 °C.
- The A-ratio of the aged MA956 samples is in good agreement with α - α' phase separation of the ferritic matrix. Higher A-ratio for PM2000 sample aged 100h indicates a mixture of α' particles and different type of scatterers.
- TEP experiments showed that the precipitation of chromium from the matrix is a more pronounced effect in the changes of Seebeck coefficient than the chromium depletion of the matrix.
- The increase of the Seebeck coefficient with the aging time corresponds very well to the results of hardness measurements in all studied materials.
- Thermal aging of the ODS materials at 650°C did not lead to an increase of the Seebeck coefficient values, but rather to a small decrease of the values.
- It is reasonable to asses the metallurgical changes of the various materials through the FWHM and BN peak shift values. In general, stronger obstacles for domain wall movement (e.g. second phase precipitates) shift the BN peak to higher values of magnetizing field while larger spectrum of defects results in a wider BN signal (higher FWHM value).
- Higher concentration of finer oxide particles, typical for as-extruded ODS materials shift the BN signal to higher values of the magnetizing field. This indicates that these defects are stronger obstacles for domain wall movement than the coarsened particles (with correspondingly lower concentration), typical for recrystallized ODS materials.
- Thermal aging of the ODS materials at 475°C leads to a new type of strong obstacles, shifting the BN signal to higher values of magnetizing field. Thermal aging at 650°C increase the peak shift only little (PM2000) or decrease the value respectively (MA956).

All four experimental techniques applied on the study of 475°C embrittlement of the high-Cr (ODS) steels showed a good sensitivity to the microstructural changes induced by thermal aging. While SANS, TEP and BN results can be directly assigned to the precipitation of new (Cr-rich) phase and can be used for complementary assessment of this process, PAS primarily reflects the thermal mobility of point defects which are, however, also related to chromium precipitation. All techniques show major changes of the measured parameters between as-received and 100hours aged samples of both, PM2000 and MA956 materials. During further aging of the materials for another 400 hours Cr-precipitation continuous at much slower rate and after 500h of thermal treatment at 475°C no more changes in the microstructure were observed. Although the results of positron lifetime measurements show certain reduction of open volume defects during the performed thermal aging, three other techniques directly confirm production of new type of defects. These defects scatter the neutron beam, change the thermal and electrical conductivity of the material and finally they act as pinning sites for the movement of magnetic domains.

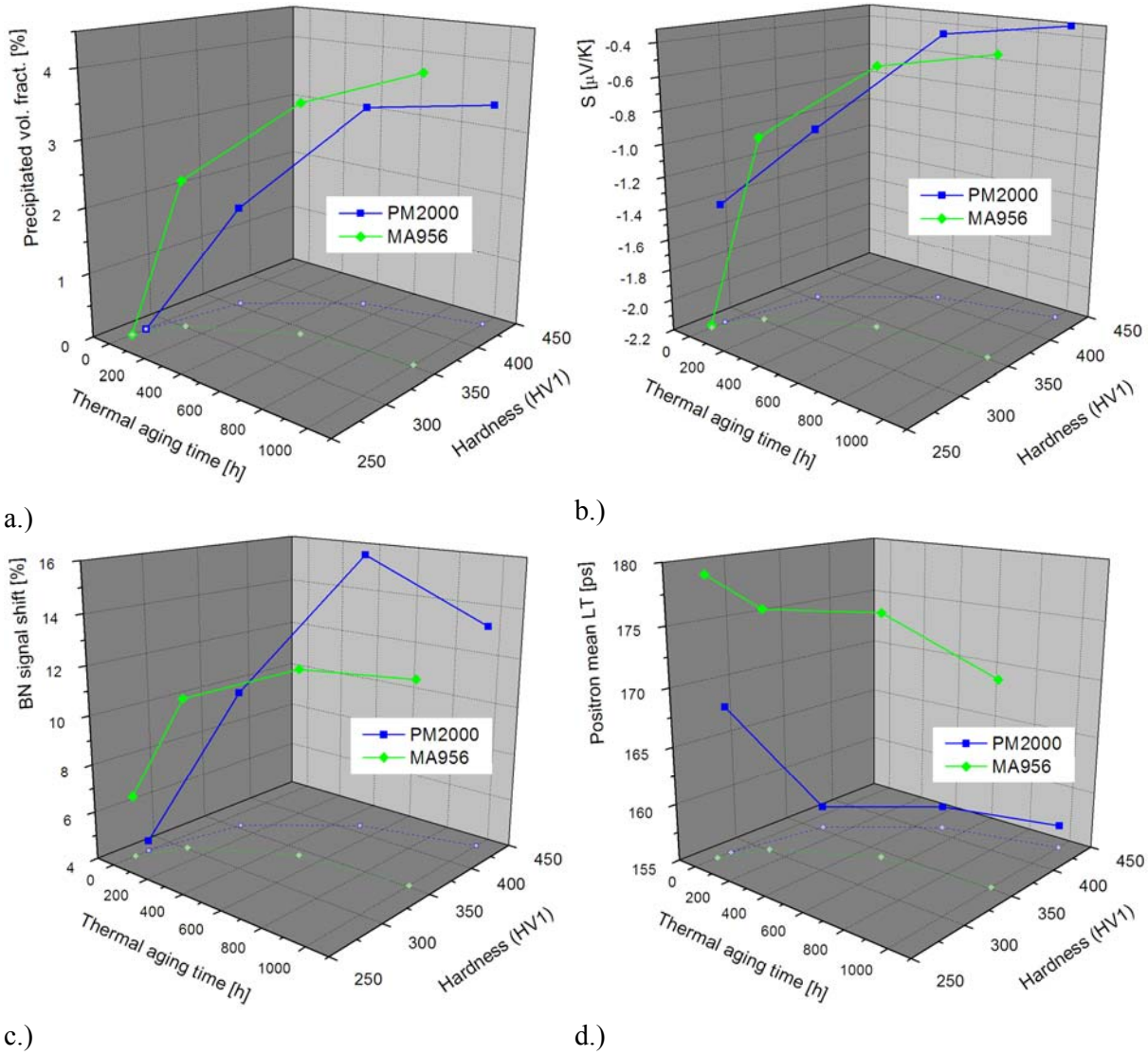

Fig. 5.1. Comparative results of the SANS (a.), TEP (b.), BN (c.) and PAS (d.) experiments plotted as a function of aging time and microhardness results.

In conclusions, we demonstrated a good feasibility of the applied techniques on the complementary characterization of the ODS steels performance. We believe that the understanding of the irradiation performance cannot be separated from the studies of thermal-induced degradation processes. In particular, irradiation experiments on ferritic ODS alloys at intermediate temperatures must be interpreted carefully and with respect to the chromium behaviour. NDT complementary techniques therefore must be thoroughly considered for the irradiation experiments in order to obtain complex information about the behaviour of material microstructure.

References:

[1.] R. L. Klueh, D. R. Harries, High-Chromium Ferritic and Martensitic Steels for Nuclear Applications, West Conshohocken, American Society for Testing and Materials, ISBN: 0-8031-2090-7 (2001).
[2.] V. Slugen et al., Journal of Nuclear Materials 302 (2002) 89-95.
[3.] V. Krsjak et al., Applied Surface Science, 255 (1) (2008) 153-156.
[4.] B. Acosta et al., Nuclear Engineering and Design 235 (2005) 1951–1959.
[5.] J. Kocık et al., Journal of Nuclear Materials 303 (2002) 52–64.
[6.] F. Bergner et al., Journal of Nuclear Materials 373 (2008) 199–205.
[7.] J. K. Sahu et al., Materials Science and Engineering A 508 (2009) 1–14.
[8.] H. K. D. H. Bhadeshia, Mater. Sci. Eng. A223 (1997) 64-77.
[9.] P. Krautwasser, A. Czyrska-Filemonowicz, M. Widera, F. Carsughi, Mater. Sci. Eng. A177 (1994) 199–208.
[10.] J. Chen, W. Hoffelner, J. Nucl. Mater. 392 (2009) 360–363.
[11.] H. Cama, T. A. Hughes, Materials for Advanced Power Engineering (monograph), in: D. Coutsouradis et al. (Eds.), Kluwer Academic Publishers, Netherlands, 1994, pp. 1497–1506.
[12.] J. Gould, J. Bernath, R. Miller, M. Alinger, C. Zanis, J. Nucl. Mater. 367–370 (2007) 1197–1202.
[13.] C. Heintze, F. Bergner, A. Ulbricht, M. Hernández-Mayoral, U. Keiderling, R. Lindau, T. Weissgärber, J. Nucl. Mater. 416 (2011) 35–39.
[14.] P. J. Grobner, Metall. Trans. 4 (1973), pp. 251-260.
[15.] M. J. Puska, P. Lanki, R. M. Nieminen, J. Phys.: Condens. Matter. 1 (1989) 6081.
[16.] M. Niffenegger, H. J. Leber, Journal of Nuclear Materials 389 (2009) 62–67.
[17.] G. R. Odette and C. Cowan, "Use of Combined Electrical Resistivity and Seebeck Coefficient Measurements to Characterize Solute Redistribution Under Irradiation and Thermal Aging," Proceedings of the 10th International Symposium on Environmental Degradation of Materials in Light Water Reactors (Houston, TX: National Association of Corrosion Engineers, 2001).
[18.] J. Degmova, L. Debarberis, Magnetic Barkhausen noise measurement of ascast model steels with parametric variation of Ni, Mn and Si content. In: Report. DG JRC, European Commission, Petten, Netherland, EUR 22512 EN (2006).
[19.] J. Veterníková et al., Nucl. Eng. Des. In Press, Corrected Proof, Available online 22 October 2011.
[20.] A. S. Wojtas, L. Suominen, B. A. Shaw, J. T. Evans, Inspection of Aircraft Landing Gear Components by Barkhausen Noise Measurement, NDT.net, Vol.3 No.9 (2006).
[21.] M. Willcox and T. Mysak, An Introduction to Barkhausen Noise and its Applications, Insight NDT Equipment Limited Technical report (2000).
[22.] D. Park, S. Park, J. Ju, K. Chang, J. Hong, J. Magn. Magn. Mater, 272-276 (2004) 1512-1514.
[23.] A. Vehanen, P. Hautojarvi, J. Johansson, J. Yli-Kauppila, P. Moser, Phys. Rev. B 25 (1982) 762.
[24.] L. C. Damonte, M. A. Taylor, J. Desimoni and J. Runco, Rad. Phys. Chem. 76 (2007) 248.
[25.] M. J. Alinger, S.C. Glade, B.D. Wirth, G.R. Odette, T. Toyama, Y. Nagai, M. Hasegawa, Mater. Sci. Eng.A 518 (2009) 150-157.
[26.] J. H. Schneibel, Z. P. Lu and S. H. Shim, "Nanoprecipitates in Steels, in "Proceedings of the Twenty First Annual Conference on Fossil Energy Materials, April 30-May 2, 2007, published December 2007, R. R. Judkins, ed., url http://www.ms.ornl.gov/fossil/proceedings.shtml, pp. 212-219.
[27.] P. Hautojärvi, C. Corbel, in: Positron Solid State Physics, Proceedings of the International School of Physics, Enrico Fermi, Course XX, Varenna, 1993.

[28.] V. Krsjak et al., Positron annihilation lifetime study of oxide dispersion strengthened steels , J. Nuc. Matter (2012), in print.
[29.] C. L. Fu, M. Miller, M. Krcmar, D. Hoelzer and C. T. Liu, TMS2007 136th Annual Meeting & Exhibition, February 25-March 1, 2007, Orlando, FL, USA, Abstract in Final Program, p. 27.
[30.] M. Miller, C. L. Fu, M. Krcmar, D. Hoelzer, C. T. Liu, Frontiers of Materials Science in China, Vol. 3, Issue 1, 2009.
[31.] R. Rajaraman, G. Amarendra, C. S. Sundar, Phys. Stat. Sol. (c) 6 (2009) 2237-2603.
[32.] O. Melikhova, J. Cizek, J. Kuriplach, I. Prochazka, M. Cieslar, W. Anwand, G. Brauer, Intermetallics 18 (2010) 592–598.
[33.] R. Paulin, R. Ripon, Appl. Phys. 4 (1974) 343–347.
[34.] Y. Ortega et al., Journal of Nuclear Materials 376 (2008) 222–228.
[35.] E. Kuramoto, S. Nagano, K. Nishi, K. Makii, Y. Aono and M. Takenaka, Mater. Sci. Forum 105–110 (1992), p. 1125.
[36.] L. Malerba, A. Caro, J. Wallenius, Journal of Nuclear Materials 382 (2008) 112–125.
[37.] O. Glatter, J. Appl. Crystallogr. 13 (1980), pp. 7-11.
[38.] Z. Berk, Food process engineering and technology, 2008, p.143.
[39.] V. A. Yardley, PhD thesis, 2003.
[40.] S. Yamaura, Y. Furuya and T. Watanabe, Acta mater. 49 (2001) 3019–3027.
[41.] T. Garstka, Journal of Achievements in Materials and Manufacturing Engineering, 27 1 (2008).
[42.] V. Krsjak et al., Journal of Physics: Conference Series 262 (2011) 012034.
[43.] V. Moorthy, B.A. Shaw, J.T. Evans, NDT&E International 36 (2003) 43–49.

European Commission
EUR 25266 – Joint Research Centre – Institute for Energy and Transport

Title: **Non Destructive Characterization of Oxide Dispersion Strengthened Steels**

Authors: Vladimir Kršjak, Zoltan Szaraz, Jozef Snopek, Peter Haehner

Luxembourg: Publications Office of the European Union

2012 – 38 pp. – 21.0 x 29.7 cm

EUR – Scientific and Technical Research series – ISSN 1018-5593 (print), ISSN 1831-9424 (online)

ISBN 978-92-79-23552-8 (pdf)
ISBN 978-92-79-23551-1 (print)

doi:10.2790/46588 (online)

Abstract

Various complementary NDT methods have been used for the characterization of oxide dispersion strengthened steels. Complex microstructure of these materials requires multi technique approach in order to better understand the effects of different nanostructures in specific environmental conditions. All techniques used in the experiment, namely positron annihilation lifetime spectroscopy (PAS), small angle neutron spectroscopy (SANS), thermoelectric power (TEP) and Barkhausen noise (BN) measurements, are sensitive to spectrum of defects in nano/micro metric range. Present report discusses feasibility of application of individual techniques on investigation of ODS materials and some degradation mechanisms. In particular, 475°C embrittlement of high-Cr ODS was studied. Precipitation of Cr-rich phase, responsible here for severe degradation of material properties, was experimentally observed by SANS as a new scattering type of ~ 2nm scattering centres in the microstructure of thermally aged materials. The same process was observed in TEP as the increase of relative Seebeck coefficient and the new precipitates were found to act as a pining site for magnetic domain wall movement by the Barkhausen noise measurement. Although the precipitation of α' phase does not change positron lifetime spectra directly, our experiments shown their non trivial effect on the lifetime parameters. Substantially different behaviour of vacancy type defects was observed in the embrittled high-Cr ODS materials, than in the 9%Cr ODS aged at the same conditions. Present results provide important guidelines for future irradiation experiments and application of the NDT on the material characterization.

LD-NA-25266-EN-N

As the Commission's in-house science service, the Joint Research Centre's mission is to provide EU policies with independent, evidence-based scientific and technical support throughout the whole policy cycle.

Working in close cooperation with policy Directorates-General, the JRC addresses key societal challenges while stimulating innovation through developing new standards, methods and tools, and sharing and transferring its know-how to the Member States and international community.

Key policy areas include: environment and climate change; energy and transport; agriculture and food security; health and consumer protection; information society and digital agenda; safety and security including nuclear; all supported through a cross-cutting and multi-disciplinary approach.

Publications Office

ISBN 978-92-79-23552-8

9 789279 235528